Published in final edited form as:
Biochemistry. 2008 September 30; 47(39): 10458–10470. doi:10.1021/bi800872d.

pH Dependence of Cyanide Binding to the Ferric Heme Domain of the Direct Oxygen Sensor from *Escherichia coli* (*Ec*DosH) and the Effect of Alkaline Denaturation†

Anil K. Bidwai, **Esther Y. Ok**, and **James E. Erman***
Department of Chemistry and Biochemistry, Northern Illinois University, DeKalb, IL 60115

Abstract

The spectrum of the ferric heme domain of the direct oxygen sensor protein from *Escherichia coli* (*Ec*DosH) has been measured between pH 3.0 and 12.6. *Ec*DosH undergoes acid denaturation with an apparent pK_A of 4.24 ± 0.05 and Hill coefficient of 3.1 ± 0.6 and reversible alkaline denaturation with pK_A of 9.86 ± 0.04 and Hill coefficient of 1.1 ± 0.1. Cyanide binding to *Ec*DosH has been investigated between pH 4 and 11. The *Ec*DosH/cyanide complex is most stable at pH 9 with a K_D of 0.29 ± 0.06 μM. The kinetics of cyanide binding are monophasic between pH 4 and 8. At pH 8.5 and greater, the reaction is biphasic with the fast phase dependent upon the cyanide concentration and the slow phase independent of cyanide. The slow phase is attributed to conversion of denatured *Ec*DosH to the native state, with a pH-independent rate of 0.052 ± 0.006 s^{-1}. The apparent association rate constant for cyanide binding to *Ec*DosH increases from 3.6 ± 0.1 M^{-1} s^{-1} at pH 4 to 520 ± 20 M^{-1} s^{-1} at 11. The dissociation rate constant averages (8.6 ± 1.3) × 10^{-5} s^{-1} between pH 5 and 9, increasing to (1.4 ± 0.1) × 10^{-3} s^{-1} at pH 4 and (2.5 ± 0.1) × 10^{-3} s^{-1} at pH 12.2. The mechanism of cyanide binding is consistent with preferential binding of the cyanide anion to native *Ec*DosH. The reactions of imidazole and H_2O_2 with ferric *Ec*DosH were also investigated and show little reactivity.

Heme proteins perform a broad spectrum of functions such as oxygen storage and transport, electron transfer, and catalysis of biological oxidations utilizing either H_2O_2 or O_2. Recently, a new class of heme proteins that serve as biological sensors has emerged (1–4). Examples in this class include the oxygen sensing proteins such as FixL[1] and the direct oxygen sensor protein from *Escherichia coli* (*Ec*Dos), nitric oxide sensing proteins such as soluble guanylate cyclase, and the carbon monoxide sensing protein, CooA (1–4).

Heme-based sensors detect the presence of small diatomic ligands such as O_2, NO or CO and initiate cellular responses to changes in the availability of the ligand. Almost all of the heme-based sensors contain two functional domains. The N-terminal heme domain is the sensor domain that binds the ligand, while the C-terminal domain is a catalytic domain that possesses

†This work was supported in part by the National Institutes of Health through grants R15 GM59740.

*To whom correspondence should be addressed. Phone: (815) 753-6867. Fax: (815) 753-4802. E-mail: jerman@niu.edu.

[1]Abbreviations: *E. coli*, *Escherichia coli; Ec*Dos, *E. coli* direct oxygen sensor full-length sequence including all domains; *Ec*DosH, heme domain of *Ec*Dos; PAS, acronym for the three proteins: Per-ARNT- Sim, which in turn are abbreviation for the *Drosophilia* period clock protein (Per), the aryl hydrocarbon nuclear transporter (ARNT), and the *Drosophilia* single minded protein (Sim); FixL, protein coded by the *fixL* gene in various *Rhizobium* species; GdHb, *Glycera dibranchiata* hemoglobin; IPTG, isopropyl-β-thiogalactopyranoside; K_D^{spec}, equilibrium dissociation constant determined from spectrophotometric titrations; K_D^{kin}, equilibrium dissociation constant calculated from the ratio of the cyanide dissociation and association rate constants; site-specific mutations are specified by the one letter codes for the amino acid residue in the wild-type protein followed by the primary sequence position and the one letter code for the amino acid residue in the mutant, thus M95A represents a mutant in which methionine at position 95 in the wild-type protein is replaced by alanine in the mutant; CT, charge-transfer bands in the optical absorption spectrum, NIR, near infrared.

catalytic or DNA-binding activity. Ligand association or dissociation from the heme triggers conformational changes that are relayed to the catalytic domain to regulate function.

*Ec*Dos was identified from sequence homology with the PAS domain of FixL (5). *Ec*Dos has an N-terminal heme-binding PAS domain, a C-terminal phosphodiesterase catalytic domainand initial studies suggested that its physiological function may be involved in the switch between aerobic and anaerobic metabolism. The optical absorption spectrum of *Ec*Dos indicates that both the reduced and oxidized forms of the heme are predominantly low-spin and hexa-coordinate. Homology modeling using the sequence and structure of the PAS domain of *Bradyrhizobium japonicum* FixL suggest that the heme ligands in *Ec*Dos are His-77 and Met-95 (6). The heme-binding PAS domain of *Ec*Dos, *Ec*DosH, has been characterized by a number of spectroscopic techniques and by x-ray crystallography (6–10). The spectroscopic properties and the crystallographic structure confirm that the heme iron is coordinated to His-77 and Met-95 in the ferrous form of *Ec*DosH. However, various spectroscopic techniques, along with studies using Met-95 mutants have produced different results for the oxidized, met form of *Ec*DosH. Magnetic circular dichroism studies in the near infrared region were used to confirm histidine-methionine coordination in met-*Ec*DosH (6). However, optical absorption, resonance Raman, circular dichroism and magnetic circular dichroism studies of met-*Ec*DosH and a number of Met-95 mutants suggest that Met-95 is not a heme ligand in the oxidized form of the protein (7,8). The x-ray structure of crystalline ferric *Ec*DosH shows water or hydroxide ion bound to the heme iron at the sixth coordination site, most likely the hydroxide ion (9). The heme environment in both the oxidized and reduced form of the protein is very hydrophobic with the heme surrounded by isoleucine, leucine, and valine residues.

Studies of the interaction of small molecules with heme proteins have often been useful in improving understanding of structure-function relationships in heme proteins. Heme proteins bind small ligands in the ferrous and ferric states. Among the ferrous heme ligands, O_2, CO, and NO are important. Takahashi and Shimizu (11) have shown that the phophodiesterase activity of *Ec*Dos is significantly enhanced upon either O_2 or CO binding to the ferrous form of the enzyme. Ferric heme ligands include cyanide, azide, fluoride and imidazole. Rates of association and dissociation of these ligands as well as their affinities provide useful clues on the effect of heme environment on the chemical reactivity of different functional classes of heme proteins.

Watanabe and coworkers (12) have investigated cyanide binding to ferric *Ec*Dos and *Ec*DosH under limited conditions and report cyanide association rate constants of 2.2 $M^{-1}s^{-1}$ for *Ec*Dos, 45 $M^{-1}s^{-1}$ for *Ec*DosH, and 500 $M^{-1}s^{-1}$ for the M95A mutant of *Ec*DosH at pH 7.5. Gonzalez *et al.* (6) found somewhat slower cyanide association rates for *Ec*DosH and its M95I mutant at pH 8, 14 $M^{-1}s^{-1}$ and 71 $M^{-1}s^{-1}$, respectively. Watanabe *et al.* (12) also report very low affinities for azide, imidazole, and fluoride binding by *Ec*Dos and *Ec*DosH.

The binding of ligands such as cyanide, azide, fluoride and imidazole to heme proteins is often pH dependent due to protonation/deprotonation of the ligand as well as to weakly acidic or basic amino acid residues in the proximal and distal heme pockets (13–23). The pH dependence of the association and dissociation rate constants, as well as the equilibrium binding constants indicate that heme proteins can discriminate between the protonated and unprotonated forms of ligands that bind to the Fe(III) heme. The general consensus in the literature is that metmyoglobin and other oxygen storage/transport proteins bind the anionic forms of the Fe (III) ligands while the heme enzymes such as the peroxidases and monooxygenases bind the neutral forms of the ligands. It is of interest to determine whether ligand binding to the heme sensors is similar to that of the oxygen transport/storage heme proteins, to the heme enzymes, or to neither of the two classical classes of heme proteins. In this study we report on an investigation of the pH dependence of cyanide binding to *Ec*DosH. We conclude that cyanide

binding to ferric *Ec*DosH is strongly affected by the apolar nature of the heme pocket and that cyanide binding is distinct from cyanide binding to either metmyoglobin or the heme enzymes.

Materials and Methods

Cloning, Expression, and Purification of EcDosH

*Ec*DosH comprises codons 1–147 of the *E. coli yddU* gene (24). *E. coli* genomic DNA was used as template to amplify this gene fragment using standard PCR technology. Primers were designed to introduce an NdeI and an EcoRI restriction site at the 5′ and 3′ ends of the amplified fragment, respectively. The amplified gene fragment was ligated into an expression vector, pET-24b(+) (Novagen), which is a T7-based vector having kanamycin as a selectable marker. The recombinant plasmid, pET-24b(+)/DosH was used to express *Ec*DosH in *E. coli*.

The plasmid pET-24b(+)/DosH was transformed into *E. coli* BL21(DE3) and a liter culture was grown at 37 °C in TB medium containing 20 μg/mL kanamycin. Expression was induced by 1 mM isopropyl-β-thiogalactopyranoside (IPTG) at OD_{600} = 1 to 1.2. The induced culture was grown overnight at 28 °C. Cells were harvested and lysed in a French press. The supernatant containing *Ec*DosH was applied to a Sephadex G-75 gel-filtration column and eluted with a buffer containing 20 mM potassium phosphate, 100 mM NaCl, pH 7.5. Fractions containing the protein were pooled and applied to a DEAE-Sepharose (FastFlow) column and eluted with a 50–500 mM NaCl gradient over 300 mL. Purity of the protein was determined by SDS-PAGE and uv-vis spectroscopy. The purity index (ratio of absorbance at the Soret maximum to that at the maximum of the protein band near 276 nm) was generally between 2.7 and 3.0.

Buffers

All buffers used in this study have an ionic strength of 0.12 M and contain a minimum of 0.020 M KCl. Buffer compositions were as follows: pH 3.0 to 3.5, 0.010 M phthalate, 0.090 M KH_2PO_4, and KCl to adjust the ionic strength; pH 4.0 to 5.5, 0.010 M acetate, 0.090 M KH_2PO_4, and sufficient KCl to adjust the ionic strength; pH 5.5 to 8.0, 0.100 M in ionic strength from KH_2PO_4/K_2HPO_4 and 0.020 M KCl; pH 8.0 to 10.0, 0.100 M Tris-HCl with sufficient KCl to adjust the ionic strength; pH 9.0 to 11.0, 0.10 M glycine and sufficient KCl to adjust the ionic strength; pH 11.0 to 12.6, 0.100 M in ionic strength from K_2HPO_4/K_3PO_4 and 0.020 M KCl, KOH was added to adjust the pH above 11.5. Because of specific ion effects in the alkaline transition region, a second series of buffers containing only potassium phosphate salts and KCl was prepared between pH 6.0 and 12.6; the potassium phosphate salts contributed 0.100 M toward the ionic strength and the remaining 0.020 M came from KCl. The buffering capacity of these buffers was low between pH 8 and pH 10 and the pH of the solutions were measured before and after each experiment when using these buffers.

Spectroscopy

A Varian/Cary Model 3E double-beam uv-vis spectrophotometer or a Hewlett Packard 8452A diode array spectrophotometer was used for optical absorption measurements. Spectra obtained on the Varian/Cary Model 3E were acquired at 1 nm resolution while those obtained using the Hewlett Packard instrument were obtained at 2 nm resolution. Band positions determined from maxima in the absorbance spectrum have uncertainties of 1 to 2 nm. Band positions for unresolved peaks, those appearing as shoulders or as minor inflections, were estimated using a peak-fitting program (PeakFit, version 4.12, SeaSolve Software, Inc. Framingham, MA). The unresolved band positions depend somewhat on peak shape and the estimates of peak position have uncertainties of about 5 nm.

Circular dichroism (CD) spectra were acquired on an AVIV Model 215 CD spectrophotometer. Protein and ligand solutions were buffered at the desired pH and the ionic strength was kept constant at 0.12 M. All measurements were done at 25°C. The concentration of ferric *Ec*DosH was determined using an extinction coefficient of 124 mM^{-1} cm^{-1} at the Soret maximum (5).

Equilibrium Constant Determinations

Spectroscopic changes associated with the formation of the cyanide complex enabled monitoring of complex formation. Determination of the equilibrium dissociation constants was done by titrating 5 to 10 μM protein with increasing concentrations of cyanide. Separate samples were prepared for each different cyanide concentration and incubated overnight in capped tubes to assure complete equilibration. The absorbance spectrum of each of the incubated solutions was determined and the equilibrium dissociation constants determined from plots of the change in absorbance, typically at 426 nm, with cyanide concentration. Equilibrium studies were carried out at integral pH units between pH 5 and 11 at 0.12 M ionic strength, 25°C.

Kinetic Measurements

Slow reactions, utilizing manual mixing, were monitored using the Hewlett Packard 8452A diode array spectrophotometer. Rapid reactions were carried out using an Applied Photophysics Ltd. Model DX.17MV stopped-flow instrument. All kinetic runs were done at 25°C.

Cyanide binding reactions were carried out under pseudo-first order conditions with excess cyanide. Observed rate constants were determined at a minimum of five different cyanide concentrations at each pH with the cyanide concentrations varying by at least a factor of five for each experiment. Total cyanide concentration varied between 1 and 50 mM depending upon the pH. A minimum of 10 individual traces of absorbance change versus time were acquired at each cyanide concentration allowing the mean value of the observed rate constant and its standard deviation to be determined. Association rate constants were determined from the slope of plots of the observed rate constant as a function of the total cyanide concentration. Kinetic studies of the association reaction were carried out at every half pH between pH 4 and 11 at 0.12 M ionic strength.

Cyanide dissociation rates were determined by removal of free cyanide from an equilibrium mixture of *Ec*DosH and KCN using gel-filtration, followed by monitoring the conversion of the *Ec*DosH/cyanide complex to free *Ec*DosH using the Hewlett Packard 8452A diode array spectrophotometer. Kinetic runs were typically initiated within ~5 min after applying the *Ec*DosH/cyanide sample to the top of the Sephadex column. During the kinetic run, complete spectra were acquired every 10 minutes for up to 20 hr. The pH of the sample was determined before and after completion of the kinetic run and the reported pH values are the average of the two determinations.

Results and Discussion

Spectroscopic Properties of Ferric EcDosH

The UV-visible spectrum of *Ec*DosH is shown between pH 5.0 and 11.8 in Figure 1. The spectra are acquired after equilibrium is achieved at each pH. Spectra between pH 5 and 9 are consistent with previously published spectra of the heme domain of *Ec*Dos (5,6,8,25–27). The spectrum is invariant between pH 5 and 8.5 and is characteristic of a predominantly hexa-coordinate, low-spin ferric heme protein. At pH 7.0, the Soret maximum occurs at 417 ± 1 nm, with maxima for the α, β, and δ bands observed at 562 ± 2 nm, 530 ± 2 nm, and 367 ± 2 nm, respectively, Table 1. In addition, there are two weak, unresolved charge-transfer bands that appear above

600 nm and two unresolved charge-transfer bands appearing between the β and Soret bands. The two long-wavelength charge-transfer bands are designated CT-1A and CT-1B and the two charge-transfer bands occurring between the β and Soret bands are designated CT-2A and CT-2B, Table 1. Figure 2 shows the visible and near infrared region of the spectrum (450 to 900 nm) acquired using high concentrations of *Ec*DosH, which includes the two long-wavelength, charge-transfer bands CT-1A and CT-1B.

The observation of two charge-transfer bands above 600 nm suggests that ferric *Ec*DosH may be a mixture of two species with different heme ligation. The position of CT-1A, near 706 nm, is reminiscent of the 695 nm band in ferric cytochrome *c* (28) and provides some support for the notion that at least a fraction of ferric *Ec*DosH has histidine-methionine coordination in solution. Hydroxy-ligated methemoglobins and metmyoglobins typically have charge-transfer bands near 600 nm while hydroxy-horseradish peroxidase has a CT band near 645 nm (29). The intensity and position of CT-1B in *Ec*DosH is similar to the charge-transfer band in hydroxy-ligated horseradish peroxidase. The crystal structure of ferric *Ec*DosH shows electron density corresponding to a water molecule (or hydroxide ion) bound to the heme iron at the second axial position (9).

Spectroscopic data are most consistent with the binding of hydroxide rather than water indicating that the heme-bound water has an abnormally low pK_A (<4). Whether the solution form of met-*Ec*DosH is a mixture of hydroxyl-ligated and methionine-ligated hemes or has only hydroxide ion bound at the second axial position, the resonance Raman spectrum is invariant to pH between pH 4 and 10 (7) and the optical absorption spectrum is invariant between 5 and 8.5, Figure 1. The unusually low pK_A is a likely consequence of the very hydrophobic nature of the heme pocket in ferric *Ec*DosH (9) and the energy requirement to stabilize a water-ligated heme group in this pocket. The ferric heme has a net positive charge due to Fe(III) binding in the dianionic core of the heme group. Binding the negatively charged hydroxide ion neutralizes the core charge on the ferric iron leading to a more stable heme complex within the hydrophobic heme pocket in *Ec*DosH.

pH Dependence of the Spectrum of EcDosH

One of the principle objectives of this study is to characterize the binding of cyanide to *Ec*DosH, especially to determine if *Ec*DosH discriminates between HCN and the cyanide anion. In order to do this, we must be able to investigate the cyanide binding reaction above pH 9 since the pK_A for the ionization of HCN is 9.04 under our experimental conditions (30). We have investigated the spectroscopic properties of *Ec*DosH over a wide range of pH in order to establish the pH stability region for this protein. The spectrum of *Ec*DosH undergoes substantial changes at acid and alkaline pH as the protein denatures. Figure 1 shows the spectroscopic changes associated with alkaline denaturation while spectra below pH 5 are shown in the Supporting Information, Figure S1. The absence of good isosbestic points in the spectra as the pH changes, Figure 1, suggests that the alkaline transition is complex. A plot of the extinction coefficient of *Ec*DosH at 418 nm between pH 3 and 12.6 is shown in Figure 3.

During investigation of the alkaline transition it was noted that slightly different spectroscopic changes occurred in buffers containing 0.10 M glycine than in buffers that did not contain glycine indicating that specific ions affected the alkaline transition (see Figure S2 in the Supporting Information). The data collected in glycine buffers are differentiated by the open symbols in Figure 3. The cause of the specific ion effect is unknown but must be associated with differential binding of phosphate and glycine to *Ec*DosH. Glycine buffers stabilize the native form of *Ec*DosH relative to phosphate buffers and the binding of at least one of these two ions must perturb the heme spectrum.

The extinction coefficient decreases sharply at low pH indicating a highly cooperative pH-dependent transition while the alkaline transition extends over a greater range of pH, whether in glycine or phosphate buffers. The pH dependence of the extinction coefficient at 418 nm was fit to eq 1 using nonlinear regression. Eq 1 allows for the possibility of cooperative pH-dependent transitions by including Hill coefficients, n_1 and n_2. The parameters E_1, E_2, and E_3 represent the limiting extinction coefficients

$$E=\frac{E_1\left(\frac{[H^+]}{K_{A1}}\right)^{n_1}+E_2+E_3\left(\frac{K_{A2}}{[H^+]}\right)^{n_2}}{\left(\frac{[H^+]}{K_{A1}}\right)^{n_1}+1+\left(\frac{K_{A2}}{[H^+]}\right)^{n_2}} \quad (1)$$

under acidic, neutral, and alkaline conditions while K_{A1} and K_{A2} are the apparent acid dissociation constants for the acidic and alkaline transitions, respectively. Best-fit values for E_1, E_2, and E_3 at 418 nm are 34 ± 4, 124 ± 1 mM^{-1} cm^{-1}, and 28 ± 2 mM^{-1} cm^{-1}, respectively. In the acid region, pK_{A1} and n_1 are 4.24 ± 0.05 and 3.1 ± 0.6, respectively. In the alkaline region, pK_{A2} and n_2 are 9.86 ± 0.04 and 1.1 ± 0.1, respectively, in phosphate buffers and 10.28 ± 0.03 and 1.0 ± 0.1, respectively, in glycine buffers. As is apparent from Figure 3, the acid transition is highly cooperative with a Hill coefficient of 3.1 while the alkaline transition can be fit to a simple non-cooperative transition. Glycine stabilizes the alkaline transition by 0.42 pH units relative to phosphate.

Reversibility of the Alkaline Transition

The beginning of the alkaline denaturation of *Ec*DosH is evident at pH 9, Figure 3, and this could interfere with the cyanide binding studies. Reversibility of alkaline denaturation would allow the cyanide binding studies to be extended to pH values greater than 9. The reversibility of the alkaline transition was investigated by incubating concentrated samples of *Ec*DosH at various alkaline pH values for 5 minutes, followed by dilution with a concentrated pH 6.5 buffer and monitoring the spectrum of the protein at timed intervals following the return of the sample to neutral pH. Figure 4 illustrates a typical experiment, in this case incubating *Ec*DosH at pH 11 for 5 minutes before returning the sample to pH ~6.5. *Ec*DosH recovers 83% of its absorbance at the Soret maximum within the time it takes to manually mix the pH 11.0-incubated sample with pH 6.5 buffer and measure the spectrum, about 10 seconds. After a 5-minute recovery period the sample recovers 97% of the absorbance at 418 nm and 100% after 80 minutes. We conclude that the alkaline transition in *Ec*DosH is fully reversible on going from alkaline to neutral pH. Additional data demonstrating the reversibility of the alkaline transition are shown in the Supporting Information, Figure S3.

Kinetics of the Alkaline Transition

We have investigated the kinetics of the alkaline transition in *Ec*DosH in both the forward and reverse direction. Up to three kinetic phases are observed during the alkaline transition, whether initiating the reaction by rapidly changing the pH of the sample from neutral to alkaline pH or *vice versa*, from alkaline pH to neutral pH. Both manual mixing and stopped-flow experiments were performed to monitor the reactions.

We define the observed rate constants as k_f^{obs}, k_i^{obs}, and k_s^{obs} where the subscripts represent the fast, intermediate, and slow phases of the reaction. Plots of the logarithm of k_f^{obs}, k_i^{obs}, and k_s^{obs} for the alkaline transition as a function of pH are shown in Figure 5. The relative amplitudes of the kinetic phases as a function of pH are included in the Supporting Information, Figure S5. The three kinetic processes indicate that a minimum of two intermediate forms of *Ec*DosH exist during the conversion of native *Ec*DosH to the final alkaline species.

A multi-component, reversible reaction is difficult to analyze (31,32). The alkaline transition involves at least four components, the native form, the denatured form, and at least two intermediates. A four component, reversible system has six possible kinetic schemes, depending upon which components are directly converted to the others (32). The simplest scheme is the sequential mechanism shown in eq 2, where N, I_1, I_2, and D 2 represent the native form of *Ec*DosH, the two intermediate

$$\mathrm{N} \underset{k_{b1}}{\overset{k_{f1}}{\rightleftharpoons}} \mathrm{I}_1 \underset{k_{b2}}{\overset{k_{f2}}{\rightleftharpoons}} \mathrm{I}_2 \underset{k_{b3}}{\overset{k_{f3}}{\rightleftharpoons}} \mathrm{D} \tag{2}$$

forms, and the denatured form, respectively. Six rate constants are required for this reaction mechanism, a forward rate constant, k_{fi}, and a back rate constant, k_{bi}, for each of the three steps, where the subscript *i* indicates the reaction step, either 1, 2, or 3. For this system of coupled, reversible reactions, each of the three observed rate constants is a complex function involving all six rate constants defined in eq 2, with the three observed rate constants given by the negative roots of a cubic equation (31). The three observed rate constants cannot be expressed in closed form, nor is there enough information to determine the values of the six rate constants defined in eq 2. The three observed rate constants are those of the normal reaction modes (33,34) as the system re-equilibrates after a pH jump. We will treat the three observed rate constants phenomenologically.

pH Dependence of the Kinetics of the Alkaline Transition

Figure 5 includes the data for both forward (solid symbols) and reverse (open symbols) pH jumps. We cannot detect the intermediate phase above pH 10.6, either because the rates of the fast and intermediate phases become too similar to deconvolute or that the amplitude of the intermediate reaction becomes too small to detect, or both. Between pH 11 and 12, the major decrease in absorption at 418 nm occurs during the fast phase of the reaction with the absorption actually increasing at 418 nm during the slowest phase of the reaction (see Supporting Information, Figure S5). This latter observation suggests that I_2 is a largely denatured form of *Ec*DosH.

All three observed rate constants are dependent upon pH, with minimum values occurring between pH 9 and 10 and increasing with increasing hydrogen or hydroxide ion concentrations. There are several ways to model the pH dependence of the observed rate constants. Since the alkaline transition has a Hill coefficient of 1 and essentially fits the titration of a single group, eq 1, we will model the alkaline transition by postulating that deprotonation of a single critical group triggers the alkaline transitions, a group with an apparent pK_A near 10. The scheme shown in eq 2 is expanded to include the protonation states of the critical group in all four protein species, eq 3. The expanded scheme also indicates that the second intermediate is a denatured form of the protein. The rate constants defined in eq 3 have a second

$$\begin{array}{ccccccc}
 & & \overset{k_{f11}}{\underset{k_{b11}}{\rightleftharpoons}} & & \overset{k_{f21}}{\underset{k_{b21}}{\rightleftharpoons}} & & \overset{k_{f31}}{\underset{k_{b31}}{\rightleftharpoons}} \\
\mathrm{HN} & & \mathrm{HI}_1 & & \mathrm{HD}_1 & & \mathrm{HD}_2 \\
pK_N \downarrow\uparrow & & pK_{I1} \downarrow\uparrow & & pK_{D1} \downarrow\uparrow & & pK_{D2} \downarrow\uparrow \\
 & & \overset{k_{f12}}{\underset{k_{b12}}{\rightleftharpoons}} & & \overset{k_{f22}}{\underset{k_{b22}}{\rightleftharpoons}} & & \overset{k_{f32}}{\underset{k_{b32}}{\rightleftharpoons}} \\
\mathrm{N} & & \mathrm{I}_1 & & \mathrm{D}_1 & & \mathrm{D}_2
\end{array} \tag{3}$$

index that distinguishes the forward and back reactions of the protonated and deprotonated states of the protein species. The acid dissociation constant of the critical group may have different values in each of the four protein species and these are indicated by pK_N, pK_{I1}, pK_{D1}, and pK_{D2}. When the critical group is protonated, the equilibria favor formation of HN, the stable native form of *Ec*DosH in the neutral pH region. When the pH is raised such that the critical group is deprotonated, the equilibria favor the denatured forms of *Ec*DosH.

In terms of the mechanism shown in eq 3, the forward and backward rates for interconversion of the various protein species will be pH dependent depending upon their state of protonation. The form of the pH dependent rate constants is given in eqs 4 and 5. The index *j* in eqs 4 and 5 can be 1, 2, or 3

$$k_{fj}=\left(\frac{k_{fj1}\frac{[H^+]}{K_{Aj}}+k_{fj2}}{\left(\frac{[H^+]}{K_{Aj}}+1\right)}\right) \tag{4}$$

$$k_{bj}=\left(\frac{k_{bj1}\frac{[H^+]}{K_{Aj+1}}+k_{bj2}}{\left(\frac{[H^+]}{K_{Aj+1}}+1\right)}\right) \tag{5}$$

depending upon the reaction step and K_{Aj} and K_{Aj+1} are the appropriate acid dissociation constants that affect the various rates, *i.e.*, K_N, K_{I1}, K_{D1}, and K_{D2}. Eqs 4 and 5 provide a template for defining a phenomenological form of the observed rate constants.

Since the reactions are reversible, the equilibration rates will involve forward and backward rate constants and the observed rate constants will have the form shown in eq 6, where the index *j* can be *f*, *i*,

$$k_j^{obs}=\frac{C_{1j}[H^+]+C_{2j}+\frac{C_{3j}}{[H^+]}}{\frac{[H^+]}{C_{4j}}+1+\frac{C_{5j}}{[H^+]}} \tag{6}$$

or *s* for the fast, intermediate, and slow phases of the alkaline transition, respectively. The coefficients, C_{1j}, C_{2j}, and C_{3j} will be complex functions of the forward and reverse rate constants and the acid dissociation constants defined in eq 3, while C_{4j} and C_{5j} will be functions of the acid dissociation constants only. Since there is no indication of saturation of any of the observed rate constants at the extremes of pH, Figure 5, the terms involving C_{4j} and C_{5j} in the denominator of eq 6 must be negligible and eq 6 can be simplified to eq 7. Eq 7 is used to fit the pH dependence of the three phases of the

$$k_j^{obs}=C_{1j}[H^+]+C_{2j}+\frac{C_{3j}}{[H^+]} \tag{7}$$

alkaline transition using non-linear least-squares regression. The best-fit values for the three coefficients, C_{1j}, C_{2j}, and C_{3j} are collected in Table 2. The solid lines in Figure 5 were calculated from eq 7 using the best-fit values for the coefficients. The slowest rate for the alkaline transition occurs at the minimum of k_s^{obs}, Figure 5. Differentiation of eq 7 with respect to $[H^+]$ indicates that the minimum rate occurs at pH 9.07 and that the half-time for the slowest phase of the reaction at pH 9.07 is 2.5 min.

Nature of the Alkaline Denatured Form of EcDosH

The UV/visible spectrum of *Ec*DosH above pH 11 (Figure 1 and Supporting Information) is very similar to that of free heme in aqueous buffer (35) suggesting a largely unfolded protein with the heme exposed to solvent. However, circular dichroism studies indicate that the polypeptide chain retains elements of secondary structure in the alkaline form of *Ec*DosH (see Supporting Information, Figure S6) while the resonance Raman studies of Sato *et al.* (7) show that the heme group remains bound to the polypeptide chain up to at least pH 10, about half way through the alkaline transition. We have additional evidence to support the conclusion that the heme remains bound to the polypeptide chain in the denatured forms of the protein and that the heme group in the alkaline denatured form of *Ec*DosH has properties that are distinct from those of free heme (see Supporting Information, Figures S7–S10).

Equilibrium Binding Studies of Cyanide to EcDosH

Upon characterization of the alkaline transitions in *Ec*DosH, equilibrium studies on the binding of cyanide were initiated. The *Ec*DosH/cyanide complex is readily formed by adding buffered solutions of cyanide to the protein. The spectrum of the *Ec*DosH/cyanide complex at pH 7.0 is shown in Figure 6 along with that of the free protein. At pH 7.0, *Ec*DosH and the *Ec*DosH/cyanide complex have similar spectra since both have hexa-coordinated low-spin heme groups. The Soret maximum of the cyanide complex is at 421 ± 1 nm and the β band is at 540 ± 2 nm, Table 1. The α band becomes less distinct in the cyanide complex, appearing as a shoulder near 568 nm. The spectrum of the *Ec*DosH/cyanide complex is essentially independent of pH between pH 4 and 11. The spectrum of the *Ec*DosH/cyanide complex at pH 11 is shown in Figure 6 along with that of the complex at pH 7 for comparison. Spectroscopic parameters are collected in Table 1. The spectrum of the *Ec*DosH/cyanide complex at pH 11 provides additional evidence that the alkaline transition in *Ec*DosH is reversible since the spectrum of the cyanide complex with free heme at pH 11 is quite different from that of *Ec*DosH/cyanide (Figure S11, Supporting Information).

The lower panel in Figure 6 shows the difference spectrum between *Ec*DosH and its cyanide complex at pH 7.0. The largest absorption change occurs near 426 to 428 nm and these wavelengths are generally used to monitor the binding of cyanide. A typical plot of the absorption change at 426 nm as a function of total cyanide concentration is shown in Figure 7 using data acquired at pH 9.0. The binding of cyanide is quite strong under the conditions of the experiment shown in Figure 7 and the absorbance change is a quadratic function of the total cyanide concentration, eq 8. P and L represent the total

$$\Delta A_{obs} = \Delta A_{\max} \frac{(B - \sqrt{B^2 - 4PL})}{2P} \quad (8)$$

protein and total cyanide concentration, respectively, and B is equal to (P + L + K_D). The data in Figure 7 were fit to eq 8 using non-linear least-squares regression in order to extract best-fit values for the equilibrium dissociation constant, K_D. Values of K_D determined from the spectrophotometric titrations are designated K_D^{spec}. K_D^{spec} was determined at each integral pH between pH 5 and 11 and the data are collected in the Supporting Information, Table S2. K_D^{spec} is pH dependent, varying from 24 ± 4 μM at pH 5.0 to a minimum of 0.29 ± 0.06 μM at pH 9.0, Figure 8. Above pH 9, in the alkaline transition region, the binding becomes weaker with K_D^{spec} increasing to 0.86 ± 0.13 μM at pH 11.

Rate of Cyanide Binding to EcDosH

The binding of cyanide to *Ec*DosH is sufficiently fast that stopped-flow techniques were required to investigate the initial phases of the reaction. Typical traces of the change in absorbance at 426 nm are shown in Figure 9. The absorbance changes are monophasic between

pH 4 and 8 and biphasic between pH 8.5 and 11. Between pH 4 and 8, the observed pseudo-first-order rate constant is designated k_{CN1} and is linearly dependent upon the cyanide concentration. Between pH 8.5 and 11, the faster of the two observed rate constants is linearly dependent upon the cyanide concentration and the equivalent of k_{CN1} at lower pH. The slower observed rate constant is independent of the cyanide concentration and designated k_{CN2}. Representative plots of k_{CN1} and k_{CN2} as functions of the cyanide concentration are shown in Figure 10.

The apparent association rate constant for cyanide binding to *Ec*DosH, k_a, can be determined from the slope of plots of k_{CN1} as a function of the total cyanide concentration as shown in Figure 10. Values of k_a are collected in the Supporting Information, Table S3. A plot of the logarithm k_a of as a function of pH is shown in Figure 11. The pH dependence of cyanide binding will be discussed below.

Slow Kinetic Phase in the Cyanide Binding Reaction

The slow, cyanide-independent phase of the cyanide binding reaction is observed between pH 8.5 and 11, within the alkaline transition region. The amplitude of this phase of the reaction correlates with the fraction of alkaline denatured *Ec*DosH present in solution, increasing from zero at pH ~8 to a maximum of 77 ± 2 % of the observed reaction at pH 10.5. The correlation breaks down at pH >11. The rate constants for the slow phase of the reaction, k_{CN2}, are collected in Table S3 of the Supporting Information. The value of k_{CN2} is independent of pH between pH 8.5 and 11, with an average value of $0.052 \pm 0.006\ s^{-1}$. This rate is similar to the intermediate phase of the alkaline transition, k_i^{obs}, Figure 5.

Rate of Cyanide Dissociation from the EcDosH/CN Complex

The rate of cyanide dissociation from the *Ec*DosH/CN complex is very slow, with a half-time on the order of hours in the neutral pH region. The dissociation rate was measured by equilibrating *Ec*DosH and cyanide at pH 9, where the binding is strongest, then removing unbound cyanide by gel-filtration. The spectrum of the gel-separated *Ec*DosH/CN complex is monitored as a function of time as cyanide dissociates from the complex to reestablish equilibrium. Passage of the *Ec*DosH/cyanide sample through the gel-filtration column also exchanges the buffer from pH 9 to a buffer of choice. The separated *Ec*DosH/CN complex equilibrates with the column buffer as it passes through the column and the measured dissociation rate is that at the pH of the column buffer. The rate of cyanide dissociation was determined between pH 4 and 12 using this technique. A typical experiment is shown in Figure 12 where the dissociation rate is determined at pH 5. At pH 5, the half-time for cyanide dissociation from the *Ec*DosH/CN complex is 1.4 ± 0.1 hr, giving a dissociation rate constant, k_d, of $(1.3 \pm 0.1) \times 10^{-4}\ s^{-1}$. Values of k_d are collected in Table S3 of the Supporting Information and a plot of the logarithm of k_d as a function of pH is shown in Figure 11.

Cyanide dissociation gives the native form of *Ec*DosH between pH ~4.5 and ~9. Below pH 4.5, the final product is acid-denatured *Ec*DosH and above pH 11, the final product is alkaline-denatured *Ec*DosH. In Figure 11, when the product of cyanide dissociation is a predominantly denatured form of *Ec*DosH, the data are shown with open symbols. An important observation is that the rate of cyanide dissociation is rate limiting during formation of the denatured forms of *Ec*DosH from the *Ec*DosH/CN complex at both pH extremes. For example, the slowest phase of alkaline denaturation at pH 12 has a rate of $0.15\ s^{-1}$ while the rate of cyanide dissociation is about two orders of magnitude slower at $2.5 \times 10^{-3}\ s^{-1}$. Likewise at pH 4.0, the rate of acid denaturation is $1.1 \times 10^{-2}\ s^{-1}$, about an order of magnitude faster than the rate of cyanide dissociation, $1.4 \times 10^{-3}\ s^{-1}$.

An equilibrium dissociation constant for the *Ec*DosH/CN complex can be calculated from the ratio of dissociation and association rate constants. This kinetically determined equilibrium dissociation constant, $K_D^{kin} = k_d/k_a$, agrees quite well with K_D^{spec}, Table S2 (Supporting Information) and Figure 8. Between pH 5 and 9, where denaturation of *Ec*DosH is not a concern, the value of K_D^{kin} averages 78% that of K_D^{spec}. Above pH 9, the alkaline denaturation of *Ec*DosH influences K_D^{spec} and K_D^{kin} to different extents. The K_D^{kin} values reported in this work are about seven times smaller (indicating stronger binding) than previously reported values calculated from the kinetic constants; 9.1 μM at pH 7.5 (12) and 4.4 μM at pH 8.0 (5, 6).

Mechanism of Cyanide Binding to EcDosH

Between pH 5 and 8, where the native form of *Ec*DosH is the dominant protein species in solution, cyanide binding appears to be a simple association reaction. At pH 8.5 and above, a second reaction appears in the cyanide binding reaction, a reaction related to the rate of interconversion of protein species within the alkaline transition region. The slow reaction segregates the protein species into two groups, those that react rapidly with cyanide and those that do not react with cyanide. For the latter group, it is more favorable to isomerize to a reactive form of the protein than to react directly with cyanide itself. A basic mechanism to rationalize cyanide binding to *Ec*DosH is shown in eq 9 where $P_{reactive}$ represents the cyanide-reactive forms of *Ec*DosH and $P_{unreactive}$ represents the cyanide-unreactive forms of *Ec*DosH. Our current hypothesis is that $P_{reactive}$ includes the

$$\begin{array}{l} P_{reactive} + CN^- \underset{k_d}{\overset{k_a}{\rightleftarrows}} P \cdot CN \\ k_i \uparrow\downarrow k_{-i} \\ P_{unreactive} \end{array} \quad (9)$$

native and first intermediate forms of the protein observed in the alkaline transition, eqs 2 and 3, while the cyanide-unreactive forms are the two denatured forms of the protein, D_1 and D_2, in eq 3. In addition, we assume that the binding of cyanide to the native and first intermediate forms of *Ec*DosH is similar since we have no evidence to the contrary. The observed rate constant for conversion of the cyanide-unreactive forms to the cyanide reactive forms, k_{CN2}, is similar to the intermediate phase of alkaline transition, k_i^{obs}, Figure 5.

An important observation is that some native *Ec*DosH exists in equilibrium with the denatured forms up to pH 11 and that the fast cyanide binding phase is the binding of cyanide to the native form of *Ec*DosH at all conditions of pH. Thus, we can measure the association rate constant for cyanide binding to native *Ec*DosH between pH 4 and 11.

pH Dependence of Cyanide Binding to Native EcDosH

The pH dependence of the logarithm of k_a, Figure 11, shows two inflections, one near pH 7 and one near pH 9, indicating that a minimum of two ionizable groups influence the binding of cyanide to the reactive forms of *Ec*DosH. The inflection near pH 9 can be attributed to the acid dissociation constant of HCN, which has a pK_A of 9.04 at 25 °C, 0.12 M ionic strength (30). The inflection near pH 7 has to be due to a group in *Ec*DosH that influences ligand binding but does not influence the spectroscopic properties of the protein, Figures 1 and 3.

A mechanism consistent with the pH dependence of both the association and dissociation rate constants for formation of the *Ec*DosH/cyanide complex is shown in eq 10. Two protonation states of

$$\begin{array}{lllll} \mathrm{HN} & + & \mathrm{HCN} & \underset{k_{-1}}{\overset{k_1}{\rightleftarrows}} & \mathrm{H_2NCN} \\ & pK_L & \uparrow\downarrow & & \uparrow\downarrow \quad pK_{C1} \\ \mathrm{HN} & + & \mathrm{CN^-} & \underset{k_{-2}}{\overset{k_2}{\rightleftarrows}} & \mathrm{HNCN} \\ \uparrow\downarrow & pK_{A3} & & & \\ \mathrm{N} & + & \mathrm{HCN} & \underset{k_{-3}}{\overset{k_3}{\rightleftarrows}} & \mathrm{HNCN} \\ & pK_L & \uparrow\downarrow & & \uparrow\downarrow \quad pK_{C2} \\ \mathrm{N} & + & \mathrm{CN^-} & \underset{k_{-4}}{\overset{k_4}{\rightleftarrows}} & \mathrm{NCN} \end{array} \tag{10}$$

the native form of *Ec*DosH, *HN* and *N*, are included in the mechanism shown in eq 10, related by an acid dissociation constant designated pK_{A3} (Note that pK_{A1} and pK_{A2} were used to describe the acid and alkaline denaturations. It is possible that pK_{A3} in eq 10 is the same as pK_N in eq 3). The mechanism shown in eq 10 allows for the binding of both HCN and the cyanide anion to both forms of the protein with unique rate constants. The acid dissociation constant for HCN is designated pK_L. Three different protonated forms of the complex must be included and these are inter-related by two ionizations characterized by pK_{C1} and pK_{C2}. Based on the mechanism shown in eq 10, the pH dependence of the association rate constant is given by eq 11. The values of k_a were fit to eq 11 using non-linear least-

$$k_a = \frac{k_1 + (k_2 \frac{K_L}{K_{A3}} + k_3)\frac{K_{A3}}{[H^+]} + k_4 \frac{K_{A3} K_L}{[H^+]^2}}{(1 + \frac{K_{A3}}{[H^+]})(1 + \frac{K_L}{[H^+]})} \tag{11}$$

squares regression and the best-fit values of the parameters are collected in Table 3. The solid line shown in Figure 11 was calculated using eq 11 and the parameters in Table 3.

The observation of the inflection near pH 9 in the plot of log k_a indicates that *Ec*DosH discriminates between the protonated and unprotonated forms of cyanide. When the pK_{A3} group is protonated at low pH, *Ec*DosH binds HCN with a bimolecular rate constant of 3.5 ± 0.3 M^{-1} s^{-1} (k_1 in eq 10 and Table 3). At high pH, when the pK_{A3} group is unprotonated, *Ec*DosH binds the cyanide anion with a rate constant of 470 ± 30 M^{-1} s^{-1} (k_4 in eq 10 and Table 3). At intermediate pH values, only upper limits can be established for k_2 and k_3. The upper limit for k_3, the binding of HCN to unprotonated *Ec*DosH, is 85 ± 13 M^{-1} s^{-1} and the upper limit for k_2, the binding of the cyanide anion to the protonated form of *Ec*DosH, is 11,000 ± 2,000 M^{-1} s^{-1}. This analysis indicates that *Ec*DosH preferentially binds the cyanide anion rather than HCN since k_4 is larger than either k_1 or the upper-limit for k_3. This contrasts with the binding of cyanide to such classic heme proteins as metmyoglobin and cytochrome *c* peroxidase where HCN binds more rapidly than the cyanide anion (15,17).

Another interesting observation concerning the pH dependence of the cyanide association rate constant is the apparent ionization near pH 7. The group with pK_{A3} 6.9 in *Ec*DosH is most likely in or near the heme pocket or possibly near the surface where cyanide enters the protein. Candidates for this group include a heme-bound water; His-77 (the proximal heme ligand), one of the two heme propionates, Asp-40 (part of the hydrogen-bonding network in the proximal heme pocket (6)), and Arg-97, which stabilizes the bound oxygen in the oxyferrous form of the protein (7). A heme-bound water can be excluded from this list of potential candidates for the group with pK_{A3} 6.9 since the spectrum of *Ec*DosH is invariant with pH between 5 and 8.5. There is ample evidence in the literature that the ionization of a heme-bound water will cause significant changes in the absorption spectrum (36) and this is not observed

in *Ec*DosH. Asp-40 can also be excluded from the list since Watanabe *et al.* (37) have investigated cyanide binding to two Asp-40 mutants and have found only minor changes in the association rate constants at pH 7.5. Arg-97 is an intriguing candidate since it does interact with, and stabilizes, the heme-bound oxygen in the oxyferrous form of the protein (10). It is possible that, upon cyanide binding, Arg-97 could reorient and stabilize the cyanide complex just as it does the oxygen complex. We will have to wait for the crystal structure of the cyanide complex to see if this occurs. One problem with associating Arg-97 with the pK_{A3} 6.9 group is the low value of the pK_A. A pK_A of 6.9 is quite low for an arginine residue although the pK_A of Arg-97 in unligated *Ec*DosH may be significantly perturbed due to interaction with two other charged groups, Arg-112 and Glu-98 (10).

The pH dependence of the cyanide dissociation rate constant is simpler than predicted by the mechanism shown in eq 10. Even though the data extend between pH 4 and 12, they do no extend far enough to determine the values of pK_{C1} and pK_{C2}. The most likely scenario is that pK_{C1} is less than 4 and pK_{C2} is greater than 12. The acid dissociation constant, K_{C1}, describes the dissociation of the proton from HCN as HCN binds to the heme iron in HP, eq 10. It is quite likely that the pK_A for HCN shifts from a value of 9 to a value <4 upon cyanide binding to the heme iron. On the other hand, pK_{C2} refers to the dissociation of a proton from HCN as HCN binds to the P, eq 10. In this case, the proton could be transferred from HCN to the pK_{A3} group in the protein. If the proton is transferred from HCN to the pK_{A3} 6.9 group, then pK_{A3} and pK_{C2} refer to proton dissociation from the same protein group, with the value of 6.9 in the free protein and a value >12 in the protein/cyanide complex. Hydrogen-bonding between the proton and the heme-bound cyanide could stabilize binding of this proton and shift the pK_A from 6.9 to >12. Since pK_{C1} and pK_{C2} are outside of the range of study, the pH dependence of k_d based on the mechanism shown in eq 10 can be simplified to eq 12. Fitting k_d as a function of pH provides

$$k_d = \frac{k_{-1}}{K_{C1}}[H^+] + (k_{-2} + k_{-3}) + \frac{k_{-4}K_{C2}}{[H^+]} \quad (12)$$

best-fit values for three parameters k_{-1}/K_{C1}, $(k_{-2} + k_{-3})$, and $k_{-4}K_{C2}$. The best-fit values are collected in Table 5 and the solid line thought the k_d data in Figure 11 is calculated from eq 12 using the values in Table 5. In the region where *Ec*DosH is stable, pH 5 to 9, k_d is independent of pH with a value of $(8.9 \pm 0.9) \times 10^{-5}$ s^{-1}. The rate of cyanide dissociation from the *Ec*DosH/cyanide complex only increases in pH regions where the protein denatures.

Comparison of Cyanide Binding in EsDosH and other Heme Proteins

A survey of cyanide binding to heme proteins shows a remarkable diversity in the kinetics of the reaction near neutral pH (see Supporting Information, Table S4 and references therein). The observed association rate constants vary by more than nine orders of magnitude, from 2.25×10^{-3} $M^{-1}s^{-1}$ for *Chromatium vinosum* cytochrome *c′* to 2.46×10^{6} $M^{-1}s^{-1}$ for spleen myeloperoxidase while the observed dissociation rate constants vary by seven orders of magnitude, from 1.4×10^{-6} s^{-1} for bovine cytochrome *c* oxidase to 22 s^{-1} for endothelial nitric oxide synthase. Studies on the pH dependence of cyanide binding indicate that heme proteins discriminate between HCN and the cyanide anion in their association reactions. The c-type cytochromes and some non-vertebrate hemoglobins preferentially react with the cyanide anion while the peroxidases and mammalian metmyoglobins preferentially react with HCN.

Cyanide binding to metmyoglobin has been studied extensively and its mechanism most thoroughly understood (38,39). At neutral pH, metmyoglobin is hexa-coordinate with a water molecule bound to the sixth coordination site of the heme iron. A small amount of penta-coordinate metmyoglobin is in equilibrium with the hexa-coordinate form. HCN diffuses into

the heme pocket and is deprotonated to form the cyanide anion. The cyanide anion reacts rapidly with the penta-coordinate metmyoglobin to form the cyanide complex. The overall association rate will be influenced by diffusional partitioning of HCN into the heme pocket, the equilibrium between hexa- and penta-coordinate forms of metmyoglobin, and the rate of deprotonation of HCN in the heme pocket. Under the typical experimental conditions, deprotonation of HCN within the heme pocket is the rate-limiting step. Studies of metmyoglobin mutants (38,39) suggest that deprotonation of HCN is affected by the polarity of the distal heme pocket and is facilitated to some extent through base-catalysis by the distal histidine. Mutant studies suggest that small ligands enter the distal heme pocket through a polar channel gated by the distal histidine residue. Association rate constants for mammalian metmyoglobins near neutral pH are typically in the range of 100 to 500 M^{-1} s^{-1} and the dissociation rate constants about 10^{-4} s^{-1}.

The peroxidases are penta-coordinate heme proteins and, as a class, react more rapidly with cyanide than any other class of heme proteins. The observed association rate constants at neutral pH are typically in the range 10^5 to 10^6 M^{-1} s^{-1} (see Supporting Information). Just as with metmyoglobin, HCN diffuses into the distal heme pocket and deprotonation of the HCN appears to be the rate-limiting step. A distal histidine residue facilitates deprotonation of HCN by base catalysis promoting the rate of association by at least two orders of magnitude (17). In cytochrome *c* peroxidase, replacement of the distal histidine with a leucine residue causes the mutant to react preferentially with the cyanide anion rather than HCN (40). The cyanide dissociation rate constants for the peroxidase are typically 0.1 to 5 s^{-1}. Although the observed rate constants for cyanide association and dissociation are both about three to fours orders of magnitude faster for the peroxidases than for the mammalian metmyoglobins, the cyanide affinity is similar between these two classes of heme proteins.

Monomeric hemoglobins that lack a distal histidine residue such as those from *Glycera dibranchiata* (41,42) react preferentially with the cyanide anion, presumably because there are no distal pocket residues to promote proton dissociation from HCN. The cyanide association rate constants are on the order of 0.3 to 2 M^{-1} s^{-1} and the dissociation rate constants are also very slow, between 10^{-5} and 10^{-6} s^{-1}, resulting in cyanide affinities similar to those of the mammalian metmyoglobins and the peroxidases.

There are few studies on the pH dependence of cyanide binding to closed-crevice heme proteins such as the cytochromes. In one of the earliest studies, George and Tsou (43) found that horse cytochrome *c* reacted with both HCN and the cyanide anion. The cyanide anion reacted preferentially with a rate constant of 15 M^{-1} s^{-1} while the HCN rate constant was 0.054 M^{-1} s^{-1}, about 300-fold slower. *Chromatium vinosum* cytochrome *c′* is a penta-coordinate heme protein but has an active site that is so sterically hindered that the cyanide association rate constant is 2.25×10^{-3} M^{-1} s^{-1}, the slowest yet reported (44). *C. vinosum* ferricytochrome *c′* preferentially reacts with the cyanide anion and the cyanide dissociation rate constant is 1.3×10^{-4} s^{-1}.

Cyanide binding studies to the ferric states of heme sensor proteins, prior to this study, have been limited to experiments done at a single pH. Cyanide binding to full length *Ec*Dos and to the isolated heme domains is slow, with association rate constants between 2.2 and 45 M^{-1} s^{-1} and dissociation constants varying from “too slow to measure” to 4.1×10^{-4} s^{-1} near pH 8 (6,12). Reported association constants for full length and the heme domain of *Sm*FixL and the heme domain of *Bj*FixL are similar to those of *Ec*Dos and range between 22 and 110 M^{-1} s^{-1} near pH 8, with dissociation rate constants varying between 1.0×10^{-4} and 4.7×10^{-4} s^{-1} (45–47).

The pH dependence of cyanide binding to *Ec*DosH (this study) is most similar to that of cytochrome *c* (43,44) and the *G. dibranchiata* hemoglobins (GdHb) components II, III, and IV (41,42) in that *Ec*DosH reacts preferentially with the cyanide anion. The pH independent association rate constants for cyanide anion binding increase in the order 12, 15, 17, 73 and 470 M^{-1} s^{-1} for GdHb-III, cytochrome *c*, GdHb-II, GdHb-IV and *Ec*DosH, respectively. For these proteins, HCN association rate constants can also be determined. The pH independent HCN association rate constants are 0.52, 0.12, 0.22, 0.33 and 3.5 M^{-1} s^{-1}, for cytochrome *c*, GdHb-III, GdHb-II, GdHb-IV and *Ec*DosH, respectively. This group of heme proteins reacts between 30 and 220 times faster with the cyanide anion than with HCN. The preference for the cyanide anion is most likely due to the difficulty in deprotonating HCN in the very nonpolar heme pockets of these proteins.

The binding of cyanide to representatives from the various classes of heme proteins display distinct mechanisms associated with the structural properties of the heme pockets. While it is likely that HCN diffuses into the heme pockets more readily than the cyanide anion, those proteins that react preferentially with HCN require a mechanism to ionize the HCN within the heme pocket. Both the peroxidases and the mammalian metmyoglobins contain distal histidines that can serve as base catalysts to promote internal HCN ionization while the invertebrate hemoglobins, the cytochromes and heme-sensor proteins lack such a residue. As a consequence, diffusion of the cyanide anion and direct binding of the cyanide anion to the positively charged heme iron in the very hydrophobic heme pocket is the preferred mechanism for cyanide binding to *Ec*DosH and the other heme-sensor proteins. Steric features and the polarity of the heme pockets in the various heme proteins cause differential diffusional barriers and differential partitioning between solvent and the heme pocket for neutral and charged ligands such as HCN and CN^- and contribute to the determination of the absolute rates of cyanide binding to heme proteins (9,38,39).

Imidazole and Hydrogen Peroxide Interaction with Ferric EcDosH

In addition to investigating the binding of cyanide to *Ec*DosH, we have also looked at two other typical reactions of ferric heme proteins, the binding of imidazole to the heme and the reaction of the heme with hydrogen peroxide. We do not detect any reaction between imidazole and *Ec*DosH using up to 1 M solutions of imidazole, consistent with a previous report (12). Likewise, *Ec*DosH does not react with hydrogen peroxide to form higher oxidation state intermediates containing Fe(IV) as do the peroxidases or metmyoglobin. At high hydrogen peroxide concentrations, oxidative degradation of the heme is observed.

Comparison of Ligand Binding to Ferric and Ferrous EcDosH

Finally, it is interesting to compare the binding of the cyanide anion to ferric *Ec*DosH with the binding of neutral diatomic ligands to ferrous *Ec*DosH. The kinetics of ligand binding to both redox states of *Ec*DosH is slow compared to other heme proteins suggesting a common feature is controlling the absolute ligand binding rates. The initial studies using cloned PAS domain of *Ec*Dos, *Ec*DosH, reported association rate constants of 2.6×10^3, 1.1×10^3, and 1.8×10^3 M^{-1} s^{-1} for O_2, CO, and NO, respectively, at pH 7 (5). Taguchi *et al.* (49) reported somewhat faster rates for *Ec*DosH at pH 8 with association rate constants of 3.1×10^4 and 7.8×10^3 M^{-1} s^{-1} for O_2 and CO, respectively. Taguchi *et al*. (49) also reported association rate constants of 1.9×10^3 and 0.81×10^3 $M^{-1}s^{-1}$ for O_2 and CO binding to full-length *Ec*Dos, respectively, at pH 8, about ten times slower than to the isolated heme domain. O_2 and CO bind to ferrous *Ec*DosH with rates that are about 66 to 17 times faster than the binding of the cyanide anion to ferric *Ec*DosH. These types of rate differences are reminiscent of the differential diffusion rates of neutral and charged ligands into a variety of proteins (50).

Supplementary Material

Refer to Web version on PubMed Central for supplementary material.

References

1. Sasakura Y, Yoshimura-Suzuki T, Kurokawa H, Shimizu T. Structure-function relationships of *Ec*DOS, a heme-regulated phosphodiesterase from *Escherichia coli*. Accounts Chem Res 2006;39:37–43.
2. Chan MK. Recent advances in heme-protein sensors. Curr Opin Chem Biol 2001;5:216–222. [PubMed: 11282350]
3. Rodgers RR. Heme-based sensors in biological systems. Curr Opin Chem Biol 1999;3:158–167. [PubMed: 10226051]
4. Gilles-Gonzalez MA, Gonzalez G, Perutz MF, Kiger L, Marden MC, Poyert C. Heme based sensors, exemplified by the kinase FixL, are a new class of heme protein with distinctive ligand binding and autoxidation. Biochemistry 1994;33:8067–8073. [PubMed: 8025112]
5. Delgado-Nixon VM, Gonzalez G, Gilles-Gonzalez MA. Dos, a heme-binding PAS protein from *Escherichia coli*, is a direct oxygen sensor. Biochemistry 2000;39:2685–2691. [PubMed: 10704219]
6. Gonzalez G, Dioum EH, Bertolucci CM, Tomita T, Ikeda-Sato M, Cheesman MR, Watmough NJ, Gilles-Gonzalez MA. Nature of the displaceable heme-axial residue in the *Ec*Dos protein, a heme-based sensor from *Escherichia coli*. Biochemistry 2002;41:8414–8421. [PubMed: 12081490]
7. Sato A, Sasakura Y, Sugiyama S, Sagami I, Shumizu T, Mizutani Y, Kitagawa T. Stationary and time-resolved resonance Raman spectra of His^{77} and Met^{95} mutants of the isolated heme domain of a direct oxygen sensor from *Escherichia coli*. J Biol Chem 2002;277:32560–32658.
8. Hirata S, Matsui T, Sasakura Y, Sugiyama S, Yoshimura T, Sagami I, Shimizu T. Characterization of Met95 mutants of a heme-regulated phosphodiesterase from *Escherichia coli*. Optical absorption, magnetic circular dichroism, circular dichroism, and redox potentials. Eur J Biochem 2003;270:4771–4779. [PubMed: 14622266]
9. Kurokawa H, Lee D, Watanabe M, Sagami I, Mikami B, Raman CS, Shimizu T. A redox-controlled molecular switch revealed by the crystal structure of a bacterial heme PAS sensor. J Biol Chem 2004;279:20186–20193. [PubMed: 14982921]
10. Park H, Suquet C, Satterlee JD, Kang C. Insights into signal transduction involving PAS domain oxygen-sensing heme proteins from the x-ray crystal structure of *Escherichia coli* Dos heme domain (*Ec*DosH). Biochemistry 2004;43:2738–2746. [PubMed: 15005609]
11. Takahashi H, Shimizu T. Phosphodieterase activity of *Ec* DOS, a heme-regulated enzyme from *Escherichia coli*, toward 3′,5′-cyclic diguanylic acid is obviously enhanced by O_2 and CO binding. Chem Letts 2006;35:970–971.
12. Watanabe M, Matsui T, Sasakura Y, Sagami I, Shimizu T. Unusual cyanide binding to a heme-regulated phophodiesterase from *Escherichia coli*: Effect of Met95 mutations. Biochem Biophys Res Commun 2002;299:169–172. [PubMed: 12437964]
13. Goldsack DE, Eberlein WS, Alberty RA. Temperature jump studies of sperm whale metmyoglobin II. Azide and cyanate binding by metmyoglobin. J Biol Chem 1965;240:4312–4315. [PubMed: 5845832]
14. Goldsack DE, Eberlein WS, Alberty RA. Temperature jump studies of sperm whale metmyoglobin III. Effect of heme-linked groups on ligand binding. J Biol Chem 1966;241:2653–2660. [PubMed: 5911637]
15. Ver Ploeg DA, Cordes EH, Gurd FRN. Comparison of myoglobins from harbor seal, porpoise, and sperm whale VII. Mechanism and catalysis for addition of cyanide to myoglobins. J Biol Chem 1971;246:2725–2733. [PubMed: 5102925]
16. Erman JE. Kinetic studies of fluoride binding by cytochrome *c* peroxidase. Biochemistry 1974;13:34–39. [PubMed: 4357655]
17. Erman JE. Kinetic and equilibrium studies of cyanide binding by cytochrome *c* peroxidase. Biochemistry 1974;13:39–44. [PubMed: 4357656]

18. Thanabal V, DeRopp JS, LaMar GN. Proton NMR characterization of the catalytically relevant proximal and distal hydrogen-bonding networks in ligated resting horseradish peroxidase. J Am Chem Soc 1988;110:3027–3035.
19. Merryweather J, Summers F, Vitello LB, Erman JE. Metmyoglobin/fluoride: Effect of distal histidine protonation on the association and dissociation rate constants. Arch Biochem Biophys 1998;358:359–368. [PubMed: 9784251]
20. Lin J, Merryweather J, Vitello LB, Erman JE. Metmyoglobin/azide: The effect of heme-linked ionizations on the rate of complex formation. Arch Biochem Biophys 1999;362:148–158. [PubMed: 9917339]
21. Taylor KC, Vitello LB, Erman JE. 4-Nitroimidazole binding to horse metmyoglobin: Evidence for preferential anion binding. Arch Biochem Biophys 2000;382:284–295. [PubMed: 11068880]
22. Bidwai A, Witt M, Foshay M, Vitello LB, Satterlee JD, Erman JE. Cyanide binding to cytochrome *c* peroxidase (H52L). Biochemistry 2003;42:10764–10771. [PubMed: 12962501]
23. Jacobson T, Williamson J, Wasilewski A, Vitello LB, Erman JE. Azide binding to yeast cytochrome *c* peroxidase and horse metmyoglobin: comparative thermodynamic investigation using isothermal titration calorimetry. Arch Biochem Biophys 2004;422:125–136. [PubMed: 14759599]
24. Blattner FR, Plunkett G III, Bloch CA, Perna NT, Burland V, Riley M, Collado-Vides J, Glasner JD, Rode CK, Mayher GF, Gregor J, Davis NW, Kirkpatrick HA, Goeden MA, Rose DJ, Mau B, Shao Y. The complete genome sequence of *Escherichia coli* K-12. Science 1997;277:1453–1474. [PubMed: 9278503]
25. Sasakura Y, Hirata S, Sugiyama S, Suzuki S, Taguchi S, Watanabe M, Matsui T, Sagami I, Shimizu T. Characterization of a direct oxygen sensor heme protein from *Escherichia coli*. Effects of the heme redox states and mutations at the heme-binding site on catalysis and structure. J Biol Chem 2002;277:23821–23827. [PubMed: 11970957]
26. Yoshimura T, Sagami I, Sasakura Y, Shimizu T. Relationships between heme incorporation, tetramer formation, and catalysis of a heme-regulated phosphodiesterase from *Escherichia coli*. A study of deletion and site-directed mutants. J Biol Chem 2003;278:53105–53111. [PubMed: 14551206]
27. Suquet C, Savenkova M, Satterlee JD. Recombinant PAS-heme domains of oxygen sensing proteins: High level production and physical characterization. Protein Expression Purif 2005;42:182–193.
28. Dragomir I, Hagarman A, Wallace C, Schweitzer-Stenner R. Optical band splitting and electronic perturbations of the heme chromophore in cytochrome *c* at room temperature probed by visible electronic circular dichroism spectroscopy. Biophys J 2007;92:989–998. [PubMed: 17098790]
29. Vitello LB, Erman JE, Miller MA, Mauro JM, Kraut J. Effect of asp-235 asn substitution on the absorption spectrum and hydrogen peroxide reactivity of cytochrome *c* peroxidase. Biochemistry 1992;31:11524–11535. [PubMed: 1332763]
30. Izatt RM, Christensen JJ, Pack RT, Bench R. Thermodynamics of metal-cyanide coördination. I pK, H°, and S° values as a function of temperature for hydrocyanic acid dissociation in aqueous solution. Inorg Chem 1962;1:828–831.
31. Rodiguin, NM.; Roodiguina, EN. Consecutive Chemical Reactions: Mathematical Analysis and Development. Van Nostrand Co.; New York, N. Y.: 1964.
32. McLaughlin E, Rozett RW. Kinetics of complex systems tending to equilibrium. Chem Tech 1971:120–121.
33. Hammes, GG.; Schimmel, PR. Rapid Reactions and Transient States. In: Boyer, PD., editor. The Enzymes, Vol II, Kinetics and Mechanism. 3. Academic Press; New York, N. Y.: 1970. p. 67-114.
34. Eigen, M.; De Maeyer, L. Theoretical Basis of Relaxation Spectrometry. In: Hammes, GG., editor. Techniques of Chemistry, Volume VI, Investigation of Rates and Mechanisms of Reactions, Part II: Investigation of Elementary Reaction Steps in Solution and Very Fast Reactions. 3. Wiley-Interscience; New York, N.Y.: 1974. p. 64-146.
35. De Villiers KA, Kaschula CH, Egan TJ, Marques HM. Speciation and structure of ferriprotoporphyrin IX in aqueous solution: Spectroscopic and diffusion measurements demonstrate dimerization, but not μ-oxo dimer formation. J Biol Inorg Chem 2007;12:101–117. [PubMed: 16972088]
36. Vitello LB, Erman JE, Miller MA, Mauro JM, Kraut J. Effect of asp-235 asn substitution on the absorption spectrum and hydrogen peroxide reactivity of cytochrome *c* peroxidase. Biochemistry 1992;31:11524–11535. [PubMed: 1332763]

37. Watanabe M, Kurokawa H, Yoshimura-Suzuki T, Sagami I, Shimizu T. Critical roles of Asp40 at the haem proximal side of haem-regulated phosphodiesterase from *Escherichia* coli in redox potential, auto-oxidation and catalytic control. Eur J Biochem 2004;271:3937–3942. [PubMed: 15373839]
38. Brancaccio A, Cutruzzolá F, Allocatelli T, Brunori M, Smerdon SJ, Wilkinson AJ, Dou Y, Keenan D, Ikeda-Saito M, Brantly RE Jr, Olson JS. Structural factors governing azide and cyanide binding to mammalian metmyoglobins. J Bio Chem 1994;269:13843–13853. [PubMed: 8188662]
39. Dou Yi Olson JS, Wilkinson AJ, Ikeda-Saito M. Mechanism of hydrogen cyanide binding to myoglobin. Biochemistry 1996;35:7107–7113. [PubMed: 8679537]
40. Bidwai A, Witt M, Foshay M, Vitello LB, Satterlee JD, Erman JE. Cyanide binding to cytochrome *c* peroxidase (H52L). Biochemistry 2003;42:10764–10771. [PubMed: 12962501]
41. Mintorovitch J, Satterlee JD. Anomalously slow cyanide binding to *Glycera dibranchiata* monomer methemoglobin component II: Implication for the equilibrium constant. Biochemistry 1988;27:8045–8050. [PubMed: 3233193]
42. Mintorovitch J, van Pelt D, Satterlee JD. Kinetic study of the slow cyanide binding to *Glycera dibranchiata* monomer hemoglobin components III and IV. Biochemistry 1989;28:6099–6104. [PubMed: 2775755]
43. George P, Tsou CL. Reaction between hydrocyanic acid, cyanide ion and ferricytochrome *c*. Biochem J 1952;50:440–448. [PubMed: 14925115]
44. Motie M, Kassner RJ, Meyer TE, Cusanovich MA. Kinetics of cyanide binding to *Chromatium vinosum* ferricy*tochrome c′*. Biochemistry 1990;29:1932–1936. [PubMed: 2158816]
45. Rodgers KR, Lukat-Rodgers GS, Barron JA. Structural basis for ligand discrimination and response initiation in the heme-based oxygen sensor FixL. Biochemistry 1996;35:9539–9548. [PubMed: 8755735]
46. Winkler WC, Gonzalez G, Wittenberg JB, Hille R, Dakappagari N, Jacob A, Gonzalez LA, Gilles-Gonzalez MA. Nonsteric factors dominate binding of nitric oxide, azide, imidazole, cyanide, and fluoride to rhizobial heme-based oxygen sensor FixL. Chem Biol 1996;3:841–850. [PubMed: 8939703]
47. Dunham CM, Diouum EM, Tuckerman JR, Gonzalez G, Scott WG, Gilles-Gonzalez MA. A distal arginine in oxygen-sensing heme-PAS domains is essential to ligand binding, signal transduction, and structure. Biochemistry 2003;42:7701–7708. [PubMed: 12820879]
48. Boffi A, Ilari A, Spagnuolo C, Chiancone E. Unusual affinity of cyanide for ferrous and ferric *Scapharca inaequivalvis* homodimeric hemoglobin. Equilibria and kinetics of the reaction. Biochemistry 1996;35:8068–8074. [PubMed: 8672511]
49. Taguchi S, Matsui T, Igarashi J, Sasakura Y, Araki Y, Ito O, Sugiyama S, Sagami I, Shimizu T. Binding of oxygen and carbon monoxide to a heme-regulated phophodiesterase from *Escherichia coli*. J Biol Chem 2004;279:3340–3347. [PubMed: 14612459]
50. Lakowicz JR, Weber G. Quenching of protein fluorescence by oxygen. Detection of structural fluctuations in protein on the nanosecond time scale. Biochemistry 1973;12:4171–4179. [PubMed: 4200894]

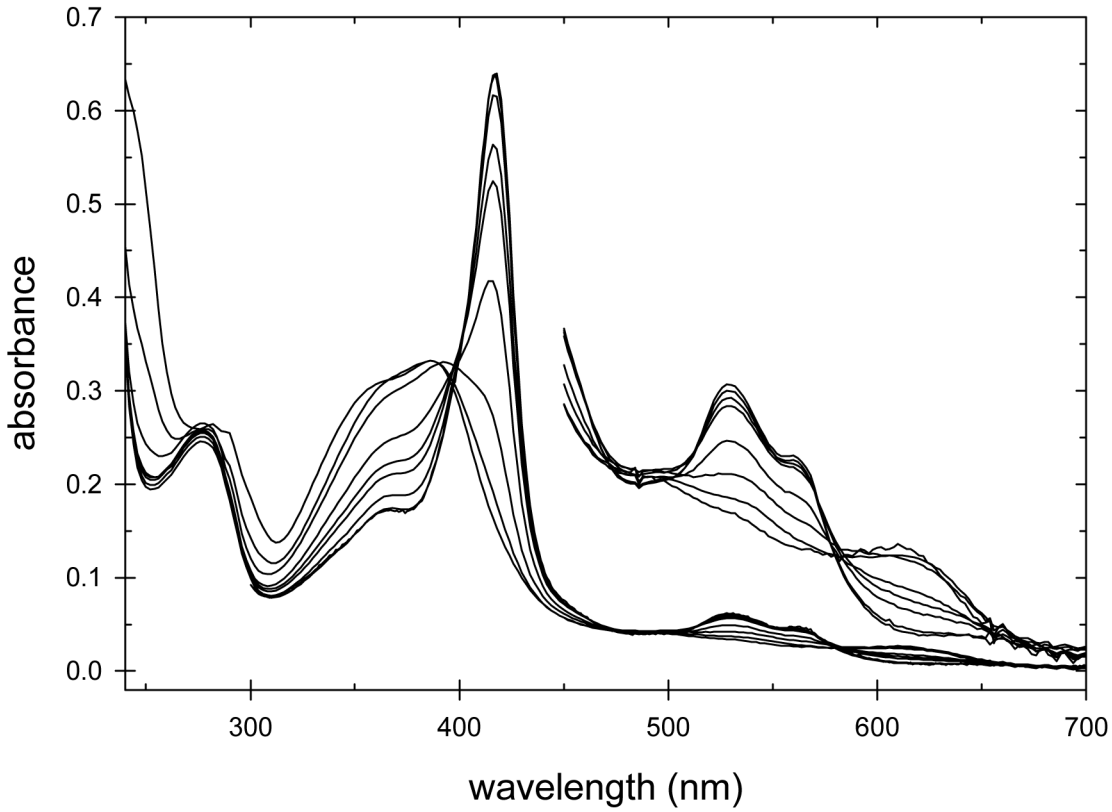

Figure 1.

pH dependence of the absorption spectrum of *Ec*DosH. The spectrum of *Ec*DosH is independent of pH between pH 5 and 8.5 with the intensity of the Soret band decreasing above pH 8.5. Nine spectra are shown with those at pH 5.00 and 6.63 essentially identical and having the highest Soret intensity. The remaining seven spectra have decreasing absorbance at 418 nm in the order pH 8.70, 9.25, 9.40, 9.70, 10.24, 10.90, and 11.78. The visible region of the spectrum is shown magnified by a factor of 5. Experimental conditions: [*Ec*DosH] = 5.15 μM, 0.12 M ionic strength buffers, 25 °C, data acquired with a Hewlett-Packard Model 4352A diode array spectrophotometer. None of the spectra shown were acquired in buffers containing glycine.

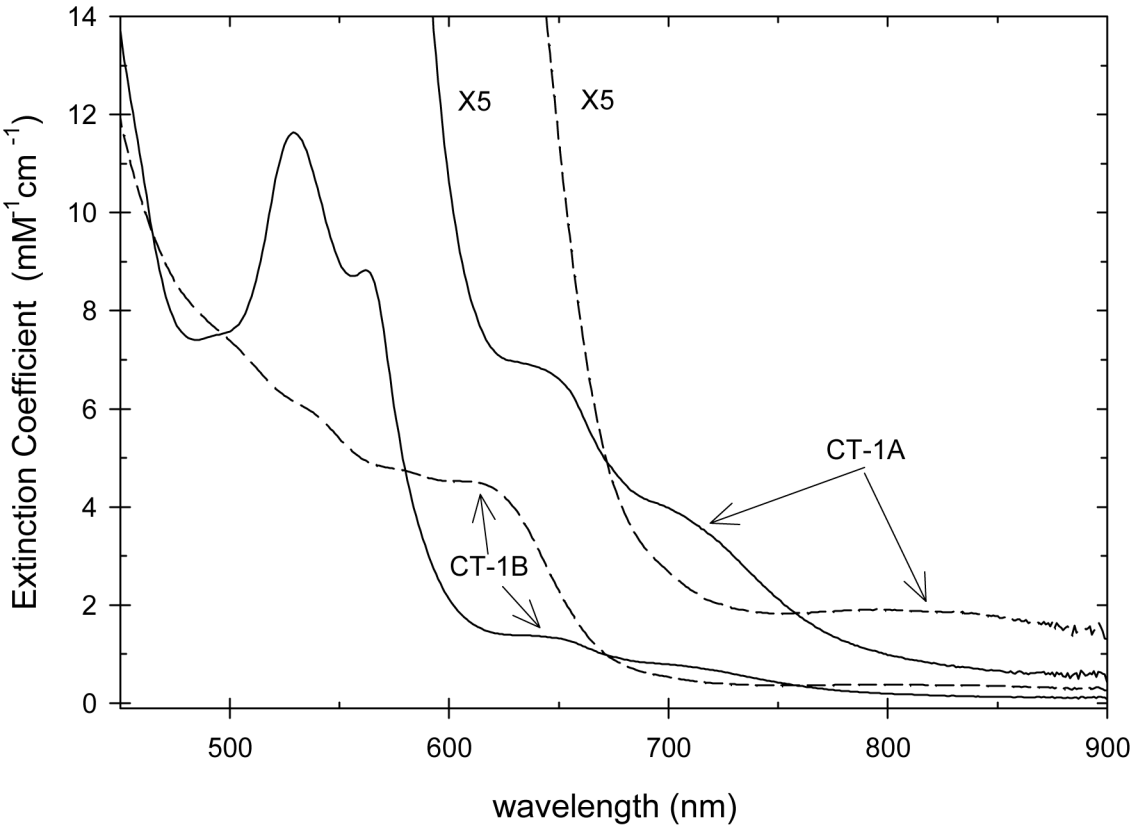

Figure 2.

Visible and near infrared (NIR) region of the spectrum of *Ec*DosH at pH 7.0 (solid lines) and at pH 11.6 (dashed lines). Between 600 and 900 nm, the spectra are also shown expanded by a factor of 5 to show the NIR charge-transfer band, CT-1A, at both values of pH. The charge-transfer bands designated CT-1B are also labeled. Experimental conditions: [*Ec*DosH] = 154 μM, 0.12 M ionic strength buffers, 25 °C, data acquired with a Varian/Cary Model 3E spectrophotometer.

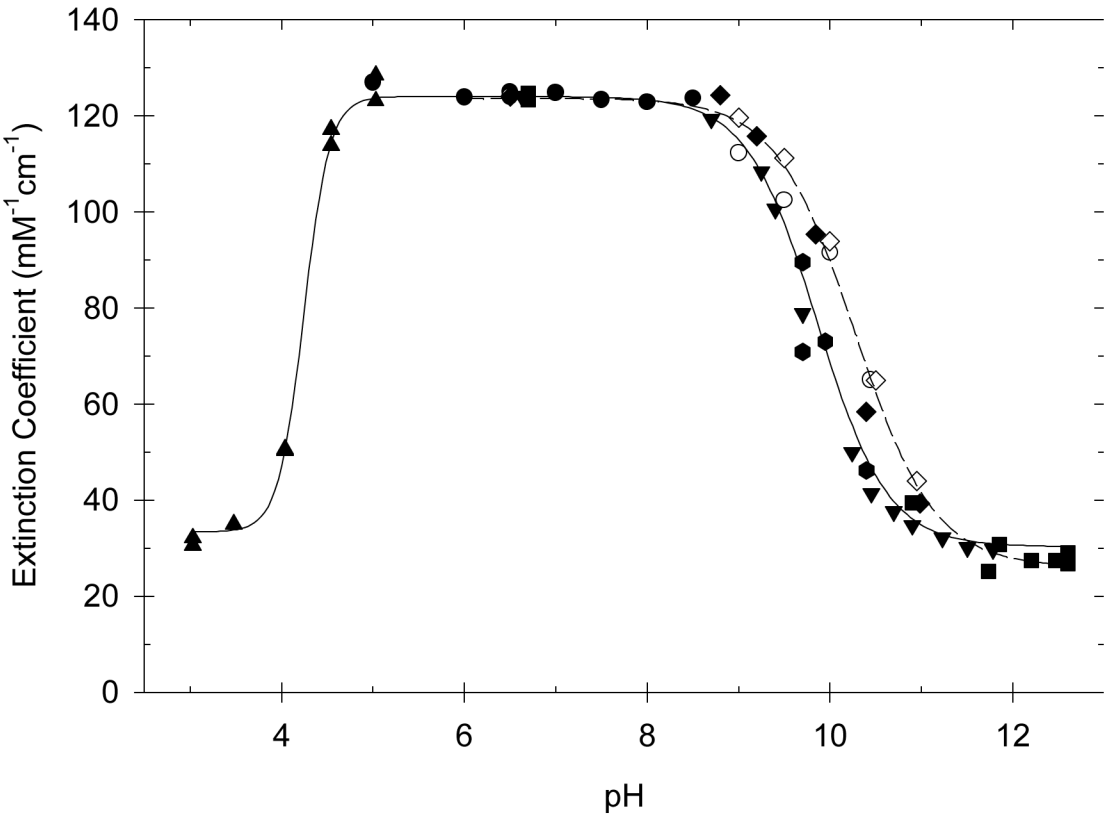

Figure 3.

pH dependence of the extinction coefficient of *Ec*DosH at 418 nm. Closed symbols indicate data acquired in buffers that do not contain glycine while the open symbols represent data obtained in buffers containing 0.10 M glycine. Different symbols indicate data acquired on different days and two isolates of *Ec*DosH were used. The data were fit to an equation involving cooperative acid and alkaline transitions (eq 1 of the text). The apparent pK_A and Hill coefficient for the acidic transition are 4.24 ± 0.05 and 3.1 ± 0.6, respectively. In buffers that do not contain glycine, the apparent pK_A and Hill coefficient for the alkaline transition are 9.86 ± 0.04 and 1.1 ± 0.1, respectively. In 0.10 M glycine buffers, the apparent pK_A and Hill coefficient for the alkaline transition are 10.28 ± 0.03 and 1.0 ± 0.1, respectively. The best-fit values for the extinction coefficients at acidic, neutral, and alkaline pH are 34 ± 4, 124 ± 1, and 28 ± 2 mM^{-1} cm^{-1}, respectively. The lines shown in the figure were calculated using the best-fit parameters. Experimental conditions: 0.12 M ionic strength, 25 °C.

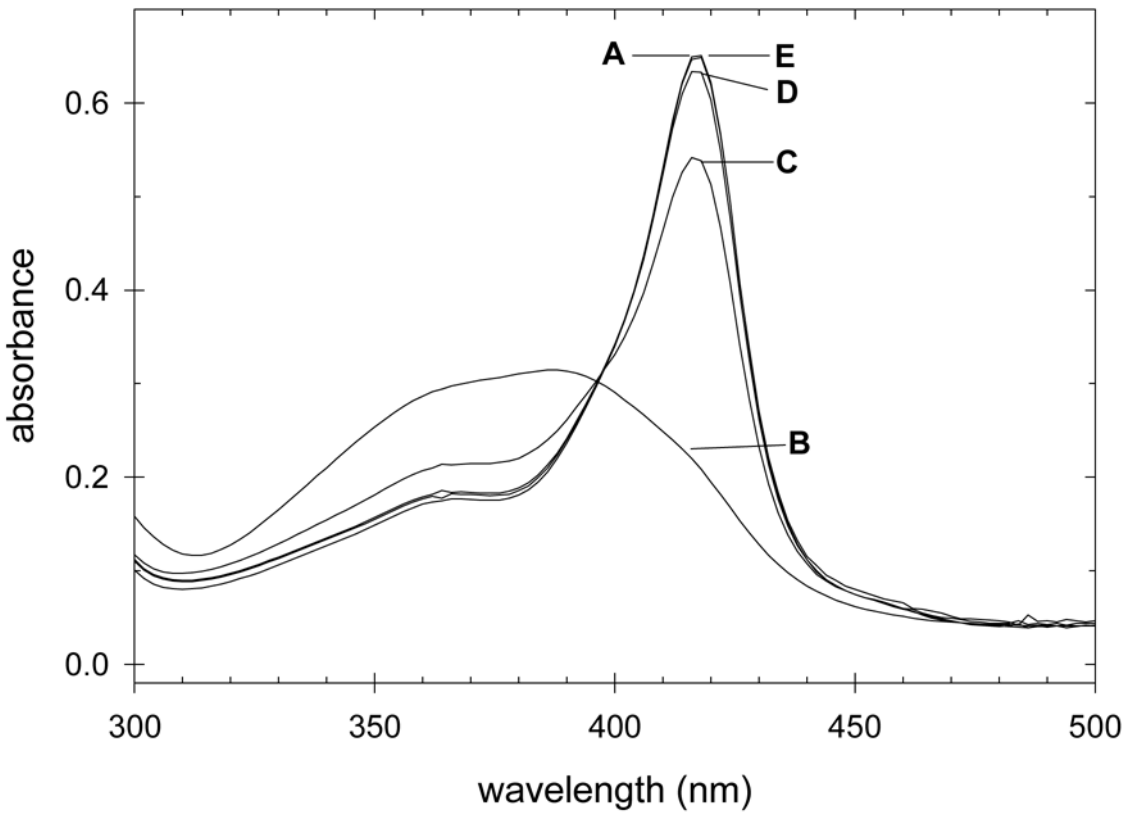

Figure 4.

Reversibility of alkaline *Ec*DosH. A. Spectrum of *Ec*DosH at pH 6.5, before exposure to alkaline pH. B. Spectrum of *Ec*DosH after incubating the sample for 5 min at pH 11.0. C. Spectrum of *Ec*DosH immediately after changing the pH from 11.0 to 6.7. The spectrum was measure within 10 s of the pH change and the sample has recovered 83% of its pre-incubation absorbance at the Soret maximum. D. Spectrum of *Ec*DosH 5 min after returning the pH to 6.7. The absorbance at the Soret maximum is 97% that of its pre-incubation value. E. Spectrum of *Ec*DosH 80 min after returning the pH to 6.7. The sample has recovered 100% of its pre-incubation absorbance at the Soret maximum.

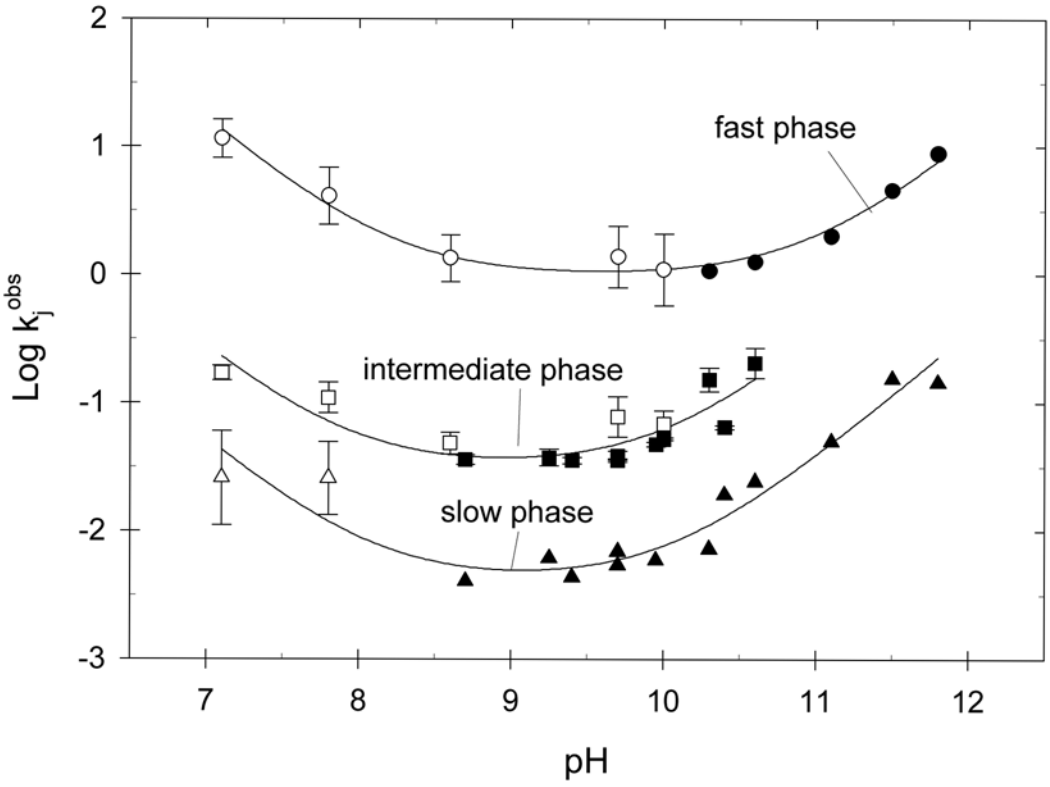

Figure 5.
pH dependence of the three observed rate constants for the alkaline transition in *Ec*DosH. Closed symbols represent data obtained from forward pH jumps while the opens symbols represent data obtained from reverse pH jumps. The solid lines were calculated from eq 7 of the text and the best-fit parameters in Table 2.

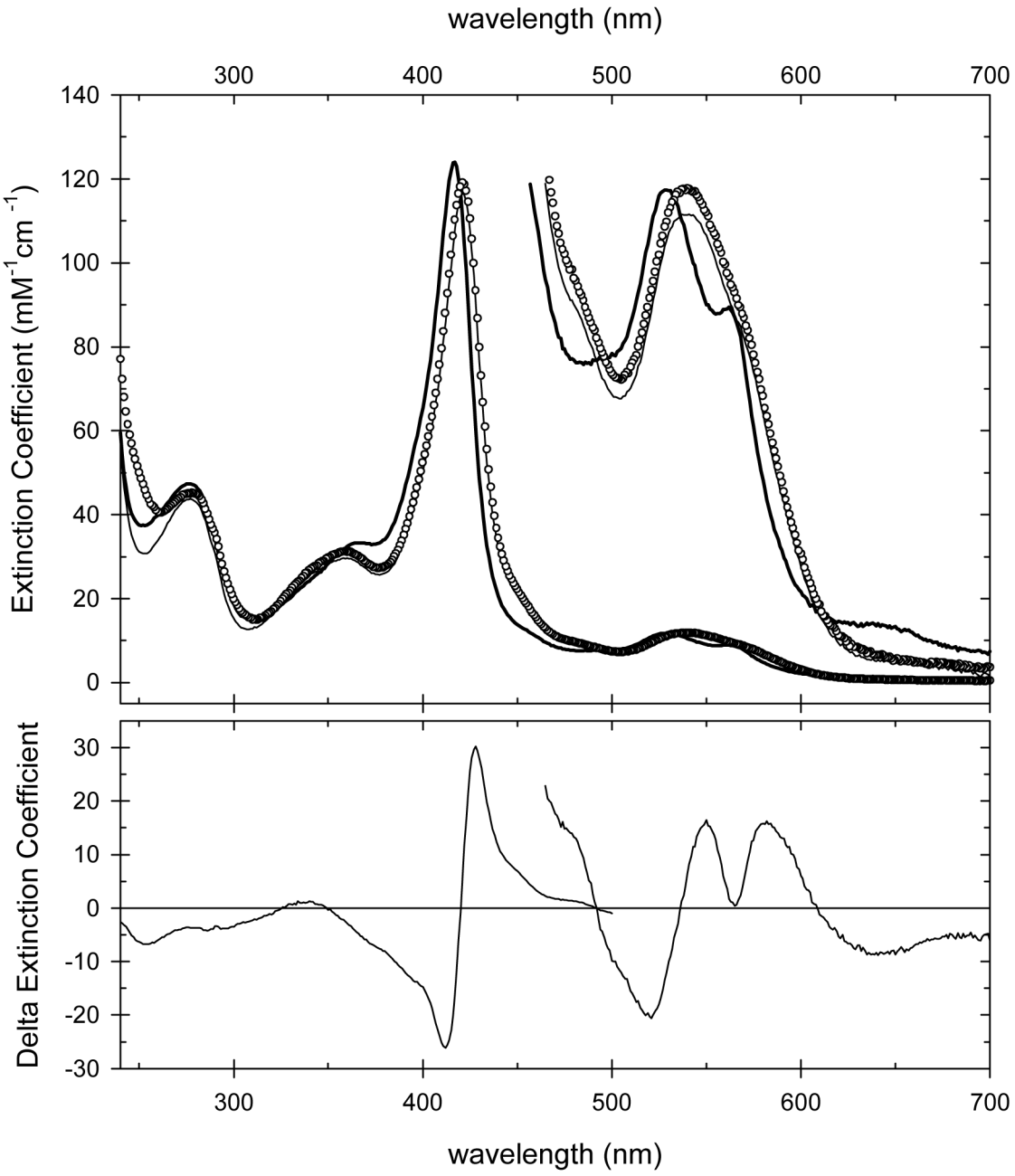

Figure 6.

Spectra of *Ec*DosH and the *Ec*DosH/Cyanide Complex. Upper Panel - *Ec*DosH at pH 7 (thick solid line) and the *Ec*DosH/cyanide complex at pH 7 (thin solid line) and pH 11 (open circles). The visible region of the spectrum is shown with the vertical axis expanded by a factor of ten. Lower Panel - Difference spectrum of the *Ec*DosH/cyanide complex minus that of *Ec*DosH at pH 7. The difference spectrum is multiplied by a factor of ten above 480 nm.

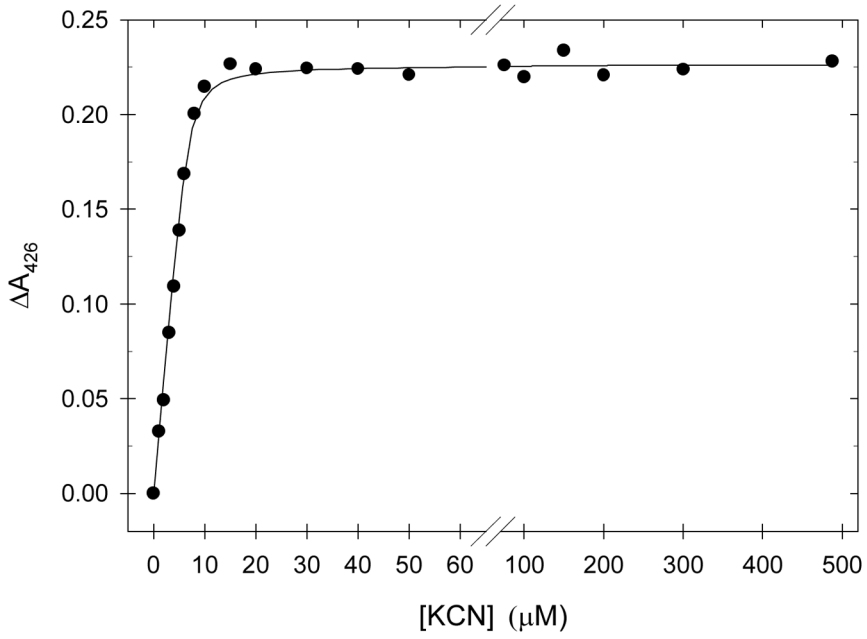

Figure 7.
Absorbance change at 426 nm for *Ec*DosH upon overnight incubations in the presence of 0 to 500 μM buffered KCN. [*Ec*DosH] = 7.2 μM, pH 9.0, 0.12 M ionic strength, 25 °C.

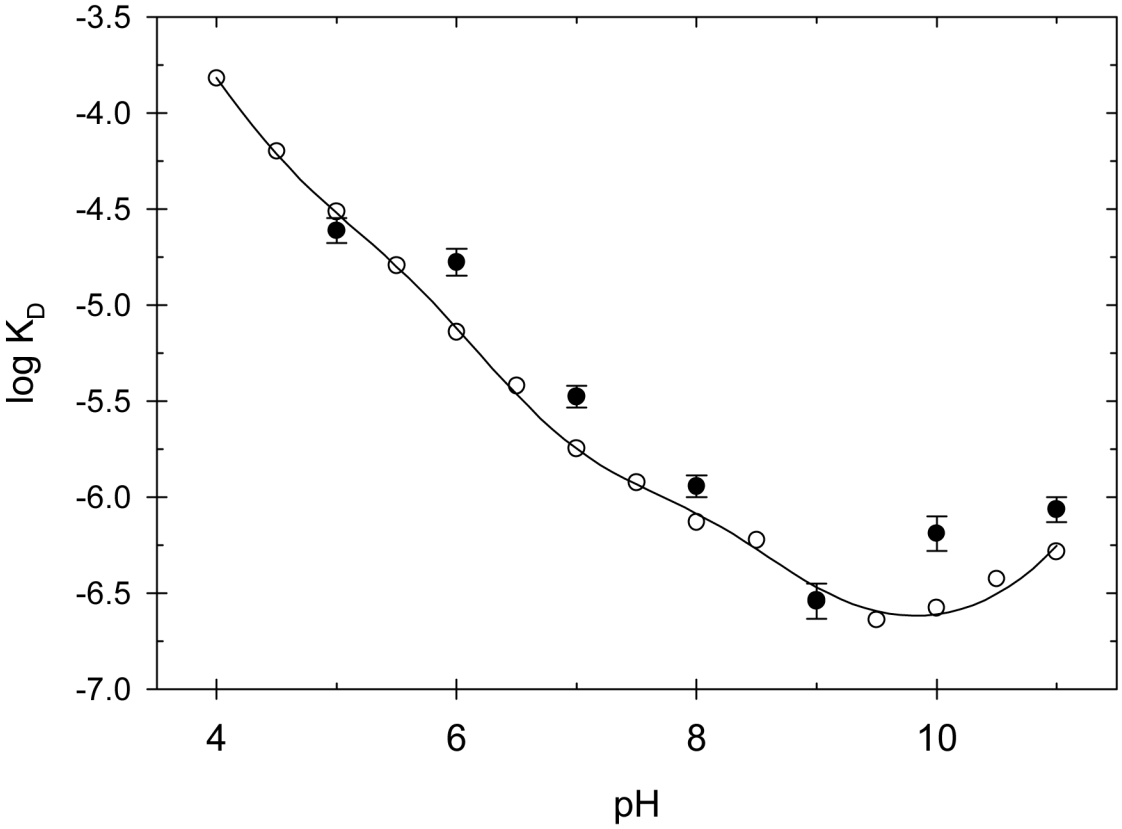

Figure 8.
pH dependence of K_D^{spec} (solid circles) and K_D^{kin} (open circles). The solid line was calculated using the ratio of dissociation (eq 12) and association (eq 11) rate constants and the best-fit parameters from Table 3.

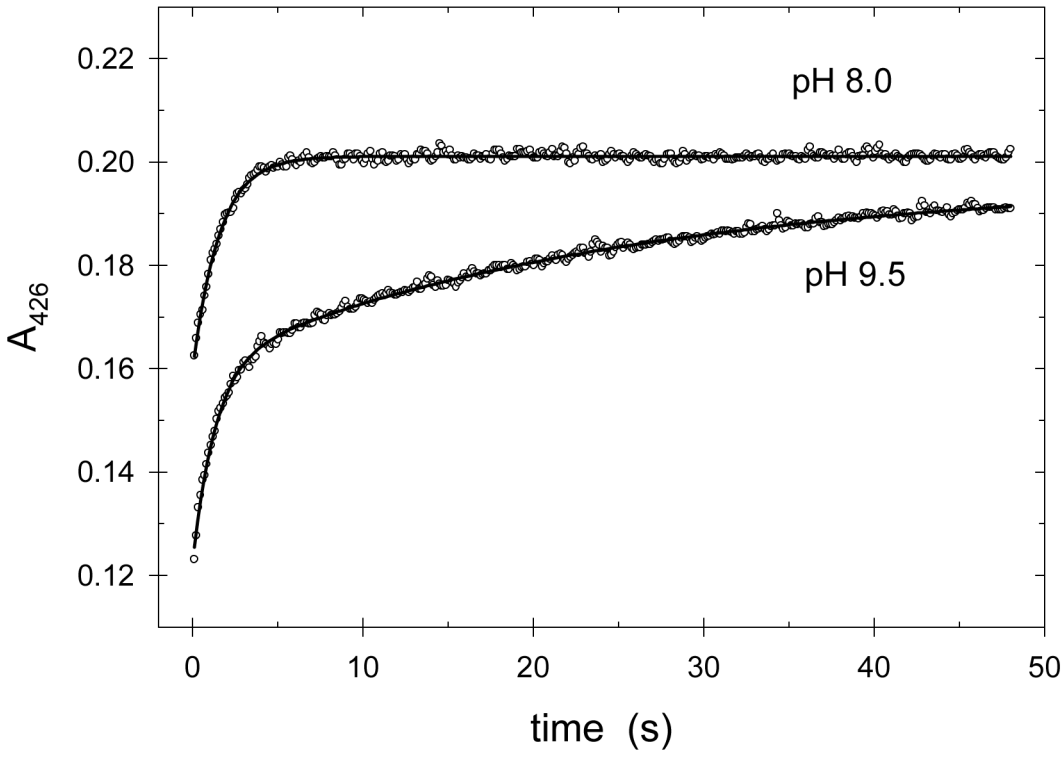

Figure 9.
Time dependence of the absorbance change at 426 nm upon addition of buffered cyanide to *Ec*DosH at pH 8.0 and pH 9.5. Experimental conditions: [*Ec*DosH] = 1.0 μM, 0.12 M ionic strength, 25 °C, [KCN] = 5 mM at pH 8.0, [KCN] = 1 mM at pH 9.5. The data at pH 8.0 fit a single exponential function with an apparent rate constant of 0.64 ± 0.1 s^{-1} while the data at pH 9.5 fit a two exponential function with apparent rate constants of 0.76 ± 0.02 s^{-1} and 0.041 ± 0.001 s^{-1}.

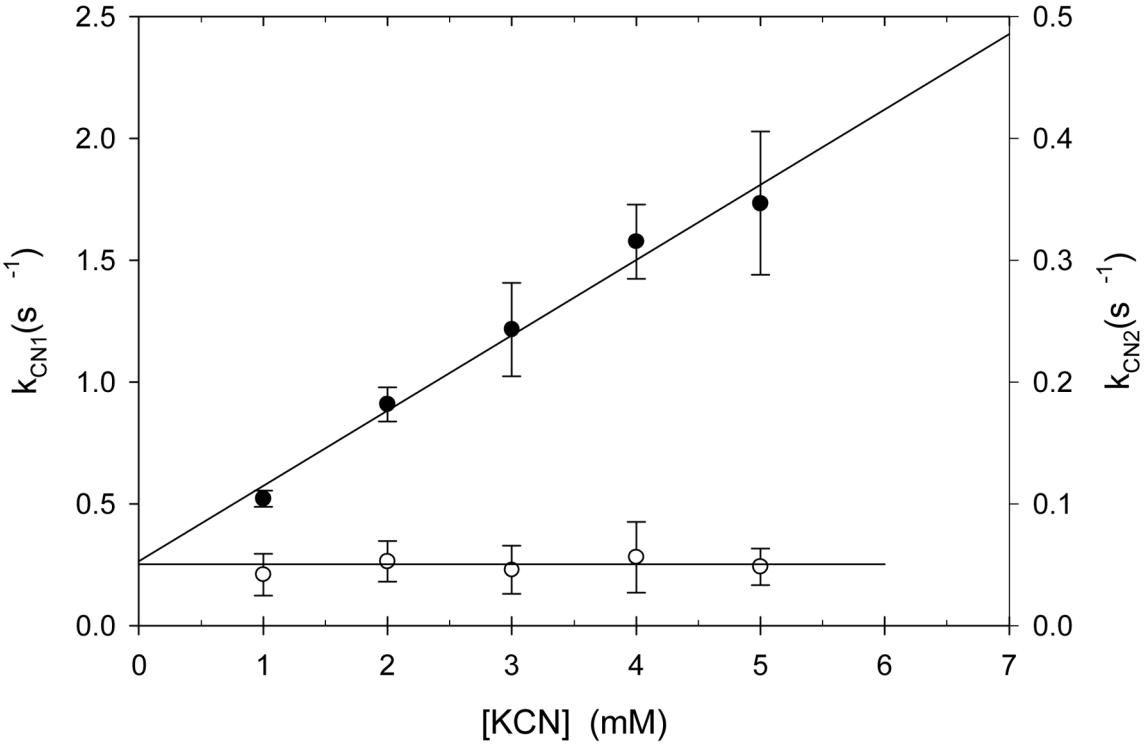

Figure 10.
Plot of k_{CN1} (solid circles - left-hand axis) and k_{CN2} (open circles - right-hand axis) as a function of the KCN concentration at pH 9.0.

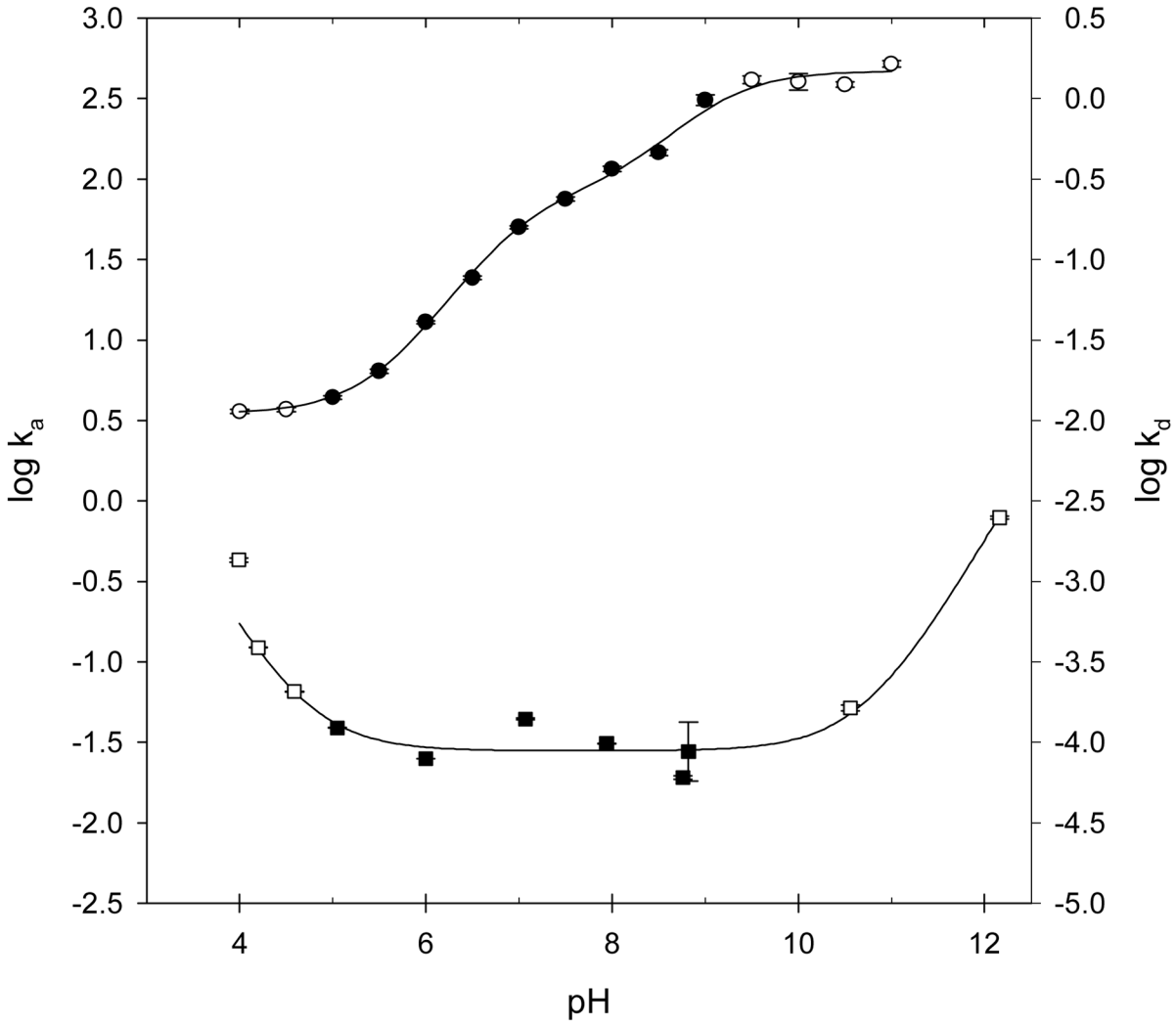

Figure 11.

Plots of the logarithm of k_a (closed and open circles) and k_d (open and closed squares) as functions of pH. The closed symbols are for the data acquired between pH 5 and 9 where the absorbance of *Ec*DosH in independent of pH. The open circles are for the data acquired at pH values where either acid or alkaline denaturation in *Ec*DosH occurs. The solid lines were calculated according to eqs 11 and 12 of the text and the best-fit parameters in Table 3.

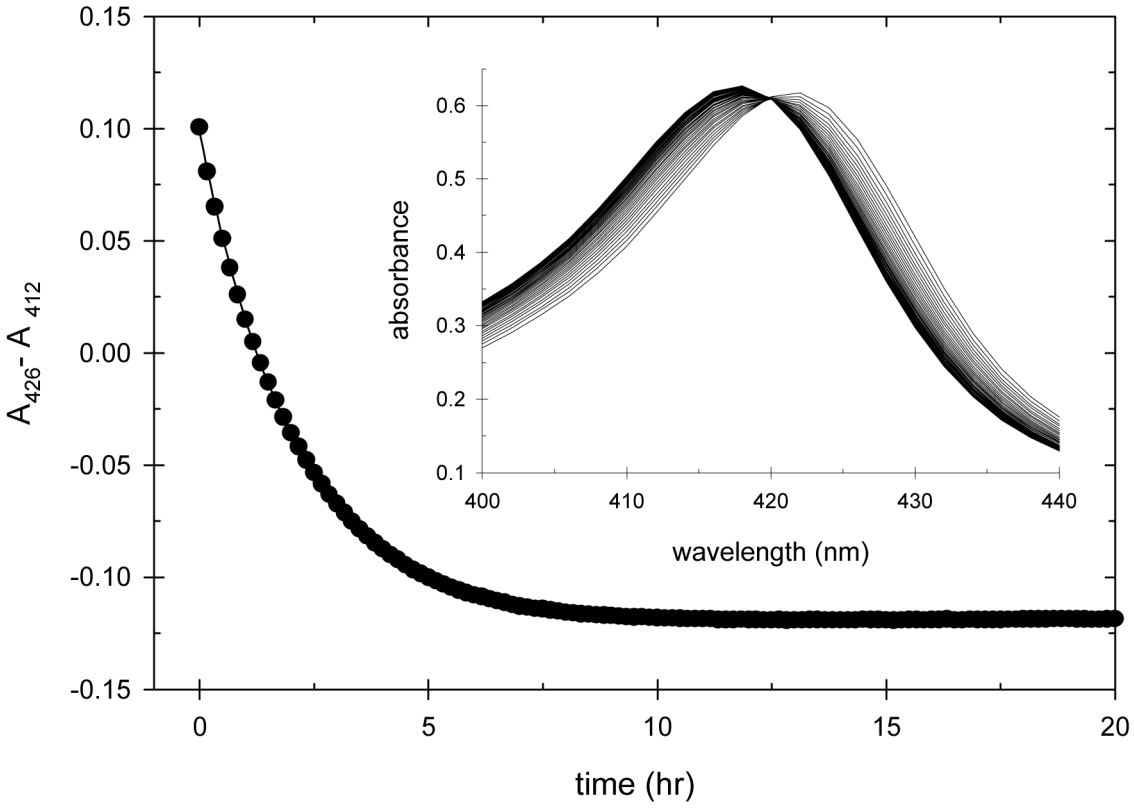

Figure 12.

Cyanide dissociation from the *Ec*DosH/CN complex at pH 5.05. The *Ec*DosH/CN complex was separated from free cyanide by passage through a Sephadex G-10 column equilibrated in pH 5.05 buffer. Spectra of the separated *Ec*DosH/CN complex were acquired every 10 minutes for a period of 20 hours using a diode array spectrophotometer. The first 60 spectra between 400 and 440 nm are shown in the inset. The *Ec*DosH/CN complex peak at 422 nm decreases and the free *Ec*DosH peak at 416 nm increases with time. To correct for instrumental drift in the single-beam spectrophotometer, the difference in absorbance at 426 nm and 412 nm was calculated and this difference is plotted as a function of time. The absorbances at 426 and 412 nm were chosen since these two wavelengths have large differences in absorbance between free *Ec*DosH and the *Ec*DosH/CN complex (see Figure 6). The difference in absorbance fits a single exponential decay equation with a first-order rate constant of 0.48 ±0.04 hr^{-1}.

Table 1

Spectroscopic parameters for *Ec*DosH and its cyanide complex at pH 7 and 11.[a]

	***Ec*DosH**		**Cyano*Ec*DosH**	
Band	**pH 7 λ (ε)nm ($mM^{-1}cm^{-1}$)**	**pH 11 λ (ε)nm ($mM^{-1}cm^{-1}$)**	**pH 7 λ (ε)nm ($mM^{-1}cm^{-1}$)**	**pH 11 λ (ε)nm ($mM^{-1}cm^{-1}$)**
CT-1A	~706*sh* (0.9)	820 ± 20 (0.4)	-	-
CT-1B	~648*sh* (1.4)	~625*sh* (4.0)	-	-
α	562 ± 2 (9.0)	~587*sh* (4.4)	~568*sh* (8.5)	~568*sh* (8.9)
β	530 ± 2 (12)	~541*sh* (5.4)	540 ± 2 (11.1)	540 ± 2 (11.8)
CT-2A	~488*sh* (7.6)	~492*sh* (7.3)	~480*sh* (9.0)	~480*sh* (9.6)
CT-2B	~449*sh* (14)	-		
Soret (γ)	417 ± 1 (124)	390 ± 2 (51)	421 ± 1 (117)	421 ± 2 (119)
δ	367 ± 2 (36)	~351*sh* (44)	360 ± 2 (30)	360 ± 2 (31)

[a]Bands that appear as shoulders in the spectra are indicated by the designation *sh* immediately following the estimated peak position.

Table 2

Best-fit values for the coefficients used to define the observed rate constants for the three kinetic phases observed during the alkaline transition in *Ec*DosH.[a]

Observed Rate Constants	C_{1j} ($M^{-1}s^{-1}$)	C_{2j} (s^{-1})	C_{3j} ($M\ s^{-1}$)
k_f^{obs}	$(1.6 \pm 0.2)\ 10^8$	0.99 ± 0.10	$(1.1 \pm 0.1)\ 10^{-11}$
k_i^{obs}	$(1.8 \pm 0.6)\ 10^6$	0.051 ± 0.011	$(3.9 \pm 1.1)\ 10^{-12}$
k_s^{obs}	$(4.9 \pm 1.8)\ 10^5$	$(4.1 \pm 1.0)\ 10^{-3}$	$(3.5 \pm 0.7)\ 10^{-13}$

[a]The observed rate constants and coefficients are defined in eq 7 of the text. The index *j* represents either *f*, *i*, or *s* for the fast, intermediate, and slow phases of the alkaline transition, respectively.

Table 3

Kinetic parameters for cyanide binding to *Ec*DosH.[a]

Parameter (units)	Value	Parameter (units)	Value
K_1 ($M^{-1}s^{-1}$)	3.5 ± 0.3	k_{-1}/K_{C1} (M^{-1} s^{-1})	4.6 ± 1.2
$(k_2\frac{K_L}{K_{A3}} + k_3)(M^{-1}s^{-1})$	85 ± 13	(k_{-2} + k_{-3}) (s^{-1})	(8.9 ± 0.9) 10^{-5}
k_4 ($M^{-1}s^{-1}$)	470 ± 30	k_{-4} K_{C2} (M s^{-1})	(1.7 ± 0.4) 10^{-15}
pK_{A3}	6.9 ± 0.1	pK_{C1}	< 4
pK_L	9.04 [b]	pK_{C2}	>12

[a] Parameters are defined in eq 14.

[b] The value of pK_L was fixed at the literature value for the HCN acid dissociation constant (30).